Simulation and Performance Analysis of Active PCM-Heat Exchanger to Optimize Building Operation

Navid Morovat

A Thesis

In the Department

Of

Building, Civil and Environmental Engineering

Presented in Partial Fulfilment of the Requirements

for the Degree of

Master of Applied Science (Building Engineering) at

Concordia University

Montreal, Quebec, Canada

March 2019

CONCORDIA UNIVERSITY

CONCORDIA UNIVERSITY

School of Graduate Studies

This is to certify that the thesis prepared

By: Navid Morovat

Entitled: Simulation and Performance Analysis of Active PCM-Heat Exchanger to Optimize Building Operation

and submitted in partial fulfillment of the requirements for the degree of

Master of Applied Science (Building Engineering)

Complies with the regulations of the University and meets the accepted standards with respect to originality and quality.

Signed by the final Examining Committee:

Dr. Fuzhan Nasiri — Chair, Examiner

Dr. Bruno Lee — Examiner

Dr. Georgios Vatistas — External Examiner

Dr. Andreas K Athienitis — Supervisor

Dr. José Agustín Candanedo — Supervisor

Approved by _____
Chair of Department of Graduate Program Director

_____
Dean of faculty

March 20th, 2019

ABSTRACT

Simulation and Performance Analysis of Active PCM-Heat Exchanger to Optimize Building Operation

Navid Morovat

This thesis presents a simulation study of an active energy storage device, intended to enhance building operation, and which is designed to be installed in the ceiling plenum of an office space, a mechanical room or in other convenient locations. This device, consisting of an arrangement of several panels of a phase-change material, may be charged or discharged as required with an air stream passing through the gaps between the panels, thus operating as a PCM-air heat exchanger (PCM-HX).

The first part of the thesis focuses on the design of the PCM-HX. Several design configurations are evaluated; investigated parameters include the PCM-HX dimensions, the number of air channels, and airflow rates. The Thesis also includes an experimental validation of the PCM model. Design criteria that were considered in the parametric study include the amount of stored heat, the time needed to charge/discharge the PCM storage and the overall energy density of the device.

The second part of the thesis evaluates different control strategies targeting reductions in peak demand and HVAC system sizing during winter. The effect of a linear ramp of room temperature setpoint and PCM-HX on peak load reduction is investigated. It was found that implementing a two hour linear ramp in temperature setpoint –together with a PCM-HX configuration with six air

channels– can reduce the heating peak load by 41%, relative to a benchmark case without the PCM-HX.

The third part of the thesis presents a simulation case study of The PCM-HX for free-cooling purposes. Results show that in the present case-study, 14% reduction in energy consumption and 24 % reduction in cooling power fluctuation (W) during daytime could be achieved using the PCM heat exchanger (PCM-HX) for free cooling.

The last section of the thesis evaluates effect of the PCM-HX on energy flexibility in building. The potential of shifting the energy use from high to low price periods is investigated. Results show that such a PCM-HX along with appropriate control strategies could provide flexibility to the grid, reduce mean power load during daytime and peak power demand. It was found that the PCM-HX could enhance energy flexibility by 10 % in winter day and 20% in summer day.

Keywords: Active PCM heat exchanger, Thermal energy storage, Performance optimization, Peak load reduction, Energy flexibility

ACKNOWLEDGEMENTS

I would like to thank my supervisors, Prof. Andreas K Athienitis and Dr. José A. Candanedo, for their precious guidance and advice. Your great supervision motivated me to continue every step successfully. You have granted me innumerable enriching experiences: Building simulation conference (eSim 2018) in École de technologie supérieure (ETS University) in April, 12th IIR Conference on Phase-Change Materials and Slurries for Refrigeration and Air Conditioning (PCM 2018) at Orford in May, IEA SHC Annex 56 and Mission Innovation in Concordia in September, and IEA EBC Annex 67 in October.

Technical support from Hydro-Quebec Laboratoire des Technologies de l'Energie Shawinigan research center under NSERC/Hydro-Quebec industrial research chair is greatly acknowledged. I would like to thank NSERC for the funding of this project through Dr. Candanedo's Discovery Grant, and the NSERC/Hydro-Québec Industrial Research Chair ("Optimized operation and energy efficiency: towards high performance buildings") held by Dr. Athienitis. I would like to thank Eric Dumont and the rest of the Hydro-Québec IREQ LTE team. I would like to thank Etienne Saloux and Arash Bastani from NRC CanmetENERGY.

I want to thank all of my colleagues within the Centre for Zero Energy Building Studies. It was very interesting and though-provoking working in a multidisciplinary team. Thank you all for your friendship, enthusiasm, helpful ideas and cooperation. Thank you Vasken Dermardiros for guiding me and providing me your experimental data and for the stimulating discussions.

I also would like to appreciate my parents and my sister for their constant supports during my studies and their encouragements to continue my studies through the best way. Finally, I would like to thank my all friends who supported me to make my studies and life more beautiful.

TABLE OF CONTENTS

LIST OF FIGURES

LIST OF TABLES

LIST OF ACRONYMS

Name	Definition
AHU	Air Handling Unit
CV - RMSE	Coefficient of Variance of Root-Mean-Square-Error
FDM	Finite Difference Method
HVAC	Heating, Ventilating and Air Conditioning
HX	Heat Exchanger
IEA	International Energy Agency
MPC	Model-based Predictive Control
NSERC	Natural Science and Engineering research council [of Canada]
PCM	Phase Change Material
SSEC	[Paul Fazio] Solar simulator-environmental chamber
TES	Thermal Energy Storage
TOU	Time of use [electrical pricing]
WWR	Window to Wall ratio

NOMENCLATURE

C_{avg}	average specific heat of PCM in the sensible range (J/$kg \cdot$ K)
C_{i}	thermal capacitance of node i (J/K)
C_{p}	specific heat (J/$kg \cdot$ K)
D_{h}	hydraulic diameter (m)
h_{conv}	heat conduction coefficient (W/$m^2 \cdot$ K)
H_{HX}	height of the PCM-HX (m)
k	heat conduction coefficient (W/$m \cdot$ K)
k_{C}	air capacitance multiplier (-)
k_{i}	integral gain (-)
k_{p}	proportional gain (-)
k_{liquid}	conductivity of the liquid phase (W/$m \cdot$ K)
k_{solid}	conductivity of the solid phase (W/$m \cdot$ K)
$\dot{m}$	mass flow rate (kg/s)
N_{DR}	diffusivity ratio (-)
Q_{heater}	auxiliary heat from an electric heater (W)
R_{ij}	resistance between node i and j (K/W)
Re	Reynolds number (-)
$skew$	skewness factor (-)
U	thermal conductance (W/K)
v	average fluid velocity (m/s)
ω	temperature range of phase change
Δt	simulation time step ($second$)

t_{PCM}	PCM layer thickness
T	temperature (℃)
T_{b}	bulk air temperature (K)
T_{surface}	average temperature of the front and back PCM surface (℃)
T_{sp}	room air setpoint (℃)
W_{HX}	width of the PCM-HX (m)

Greek letters

ρ	Density (kg/m^3)
ω	Temperature range of phase change

Dimensionless Numbers:

$$\mathrm{Re} = \frac{\text{inertial forces}}{\text{viscous forces}} = \frac{\rho v D_h}{\mu}$$

$$\mathrm{Nu} = \frac{\text{convective heat transfer}}{\text{conductive heat transfer}} = \frac{h D_h}{k}$$

$$\mathrm{Pr} = \frac{\text{viscous diffusion rate}}{\text{thermal diffusion rate}} = \frac{C_p \mu}{k}$$

$$\text{where: } D_h = \frac{4 \cdot \text{cross sectioal area}}{\text{wetted perimeter}} = \frac{4 \cdot A}{P}$$

1. Chapter 1

Introduction

This chapter includes: the background and research motivation, a literature review, a conceptual summary, and finally objectives of the study and outline of the chapters that follow.

1.1. **Background**

The role of buildings as flexible loads is becoming more important; they can act as energy generators, energy storage, or/and controllers of demand (D'Angiolella, de Groote et al. 2016).

In this regard, the Annex 67 of the IEA Energy in Buildings and Communities Programme (IEA-EBC) defined energy flexible buildings as those with "the ability to manage [their] demand and generation according to local climate conditions, user needs and grid requirements" (Jensen, Marszal-Pomianowska et al. 2017).

Increasing energy flexibility for the design of smart energy system and buildings is influenced by four important factors (Reynders 2015):

- physical characteristics of the building
- HVAC systems and storage equipment

- adequate control systems and strategies
- comfort requirements

In this context, thermal energy storage (TES) along with appropriate control strategies is a key factor to increase the energy flexibility of a building by reducing the mismatch between supply and demand for heating or cooling (Zhu, Ma et al. 2009, Tabares-Velasco, Christensen et al. 2012, Klein, Herkel et al. 2017).

1.2. **Thermal energy storage**

Thermal Energy Storage (TES) is one of the most essential factors toward achieving better efficiency in buildings (e.g. Solar applications), and for heat/cool energy management in buildings due to mismatch between energy generation and use (Stritih, Tyagi et al. 2018). TES can fill the gap between energy generation and demand, and enhance the total use ratio of thermal energy (Zhu, Hu et al. 2014, Bozkaya, Li et al. 2017). Another application of TES in building is free-cooling of buildings. In free cooling, a natural resource for air conditioning in buildings will be used.

Advantages of implementation of TES in an energy system are (Dincer and Rosen 2002):

- increase of the overall efficiency and reliability
- better economic feasibility
- reducing investment and running costs
- and less pollution of the environment and less CO2 emissions

Different methods for storing Thermal energy are available: sensible heat, latent heat and thermochemical energy storage (Cabeza 2008). In *Sensible storage*, energy is stored by changing

the temperature of a storage medium (such as water, air, concrete and etc.). In this method, the amount of energy stored is depending on the temperature difference, the mass, and the heat capacity of the TES (Eq. 1):

$$Q = m \cdot C_{\mathrm{p}} \cdot \Delta T \quad (1)$$

where

- m: the mass of storage material, (kg)
- C_p: the specific heat of the storage material, (J/ (kg·°C))
- ΔT: the temperature gradient, (°C)

In *latent heat storage,* energy is stored through a phase transition (e.g. solid-liquid). In building application the solid-liquid phase change is used because of its high enthalpy and lack of pressure problems. During melting/solidifying phase, the material maintains in a constant temperature (phase change temperature). The amount of heat stored during phase change can be calculated by Eq. (2):

$$Q = m \cdot \Delta h \quad (2)$$

where

- Δh: the phase change enthalpy (also called melting enthalpy or heat of fusion), (J/kg)
- m: the mass of storage material, (kg)

1.3. **Phase change material for enhanced building flexibility**

Energy flexibility in buildings and adequate control of this flexibility are two important factors for the design of smart energy system and buildings. In this context, thermal energy storage in building components can be a key contributor to energy flexibility; phase change materials (PCM)

can be used for this purpose (Mao, Pan et al. 2017, Mao, Song et al. 2017). PCMs are a promising technology based on the principle of latent heat thermal energy storage (LHTES), whereby PCMs absorb or release large amounts of energy at a certain temperature during the phase change transition period (charging and discharging process), on account of the high heat of fusion (Du, Calautit et al. 2018).

PCMs have the benefit of facilitating the storage of passive solar gains and other heat gains, as well as heating energy and cooling energy from the HVAC system (Zhou, Zhang et al. 2015). In latent heat storage systems, energy charge and discharge normally occurs within a narrow temperature range (the transition zone) (Paris, Falardeau et al. 1993). By reducing zone temperature fluctuations, PCMs can reduce energy usage, improve thermal comfort and reduce and/or shift the electricity peak demand (Soares, Costa et al. 2013, Bourne and Novoselac 2015, Yu, Huang et al. 2015). Their integration in multilayer walls and ceilings reduces the effect of external thermal conditions on the thermal state of the building (Pasupathy and Velraj 2008, Berardi and Soudian 2018). Given the large variety of available PCM materials with different thermal properties, they can be used in multiple applications because of their wide range of latent heat storage capacities and phase change temperatures. However, for direct building applications, only PCMs having a phase transition close to human comfort temperature (about 20°C) can be used (Fleischer 2015, Heier, Bales et al. 2015).

1.4. **Passive and Active PCM applications**

PCM applications can be classified in two main categories: passive systems and active systems (Zhu, Ma et al. 2009, Gil, Medrano et al. 2010). In *passive* applications, PCMs are integrated into building envelopes to increase the effective thermal storage capacity, thus improving temperature

regulation (Childs and Stovall 2012, Bigaila and Athienitis 2017). Passive systems are charged/discharged without any mechanical heating/cooling. Passive systems use solar radiation, natural convection or temperature difference. For example, Athienitis, Liu et al. (1997) studied a test-room with a PCM-impregnated gypsum board with a particular interest in peak load shifting and solar energy utilization. Passive PCM applications can be particularly beneficial in lightweight constructions with low thermal inertia (Farid, Khudhair et al. 2004): a well-known issue in these buildings is the presence of large temperature fluctuations (Soares, Reinhart et al. 2017). This is a common problem in some cold climate regions where buildings are built with wood frame construction and large amounts of insulation to reduce heating loads. In a passive PCM installation, the PCM will typically melt during the daytime to store heat gains (solar and otherwise); the material will then solidify gradually during the nighttime thus releasing heat to the space. This process will reduce room overheating during the daytime in warm months and may decrease the need for space heating during the nighttime in the winter (Bastani, Haghighat et al. 2015, Nikoofard, Ugursal et al. 2015, Guarino, Athienitis et al. 2017).

Active thermal energy storage systems employ a PCM within a stand-alone container or device, which can be melted or solidified as required by using an external heating or cooling source. Active storage system is mainly based on forced convection heat transfer. This could be through the storage material or through a heat exchanger (e.g. a solar receiver). Active PCM systems can provide the following advantages:

- **Flexibility in heat transfer area**. The heat transfer area can be increased by adjusting the ratio of the surface area to the volume of the PCM and flow rate of the air.

- **Steady conditions for charging/discharging energy**. The high energy density of PCM

and the fact that the latent heat transfer process is approximately isothermal result in smaller temperature variations. Active thermal energy storage allows charging/discharging even when indoor conditions are steady, thus facilitating the control of thermal energy.

- **Adjustment of the melting point of the PCM**. In an active installation, it is easier to adjust the melting point (for example, by using a different material). Therefore, the range of conditions that are useful for charging/discharging the PCM can be extended.

- **Integration with mechanical systems**. With mechanical ventilation, enough airflow can be provided to achieve the desired energy storage, peak demand reduction, and load shifting. This peak demand reduction also allows for smaller heating and cooling equipment and ducts, thus saving space in buildings and capital cost.
- **Applications in retrofit projects**. Active installations are suitable for retrofits in buildings with low thermal mass since they can add significant controllable and "dispatchable" thermal energy storage.

Active systems are subdivided into two categories: (1) direct and (2) indirect systems. In a direct system, the heat transfer fluid works also as the storage medium, while in an indirect system, the heat transfer fluid passes through the storage only for charging and discharging a storage material.

Mosaffa et al. (Mosaffa, Ferreira et al. 2013) described an active PCM system intended for free cooling. This device consisted of panels separated by air gaps which enabled air to flow through the PCM. The present study investigates a similar (though not identical) system, designed to control the thermal load of an office space.

1.5. **Applications in retrofit projects**

Buildings are responsible for near 40 % of total energy and approximately 40 % of total CO_2 emission (direct and indirect) in developed countries. The prediction for building energy demand shows a 179% increase in heating and cooling energy use by 2050 compared to 2010 (Berardi and Manca 2017). In Canada, although space heating is the highest energy demand in buildings, the energy demand for space cooling continues to increase and is more than three times since 1990 (NRCan 2006).

In general, policies and initiatives have often concentrated on improving the efficiency of new buildings (Waide, Amann et al. 2007). In the meantime, the energy retrofit of existing buildings is important to achieve a reduction in the energy demand of buildings and increase the thermal comfort for occupants (Touchie, Pressnail et al. 2014).

Addition of thermal storage units in ventilation systems (e.g. air ducts or air handling units) is interesting for building retrofitting, because its implementation is not at the core of the building. The use of PCMs as a form of LHTES has gained some popularity as an optimal choice for retrofit applications (Ascione, Bianco et al. 2014, Bourne and Novoselac 2015, Guarino, Athienitis et al. 2017). This is due to the higher heat storage capacity in small volumes of PCMs and to the possibility to apply them as discreet retrofit measures (Soares, Costa et al. 2013).

In this study, a PCM-HX is presented with application for both new building and retrofit projects, in order to reduce peak load and HVAC system size. Based on the significant results of recent researches–both passively in building envelopes and actively coupled with the HVAC system– (Bastani, Haghighat et al. 2015, Kośny 2015, Narain, Jin et al. 2015, Nikoofard, Ugursal et al. 2015, Navarro, de Gracia et al. 2016, Bigaila and Athienitis 2017, Guarino, Athienitis et al. 2017,

Saffari, de Gracia et al. 2017, Soudian and Berardi 2017), the incorporation of the active PCM-HX device is investigated.

Despite wide range of studies about PCM applications in lightweight buildings (Soares, Reinhart et al. 2017), several studies have investigated the addition of PCMs to high mass buildings (Rodriguez-Ubinas, Arranz et al. 2013, Ascione, Bianco et al. 2014, Soares, Reinhart et al. 2017). Results of these studies show positive advantages that PCMs provide in high thermal mass buildings.

1.3- Overview of the thesis and objectives

Most previous research (Kuznik and Virgone 2009, Bastani, Haghighat et al. 2015, Dermardiros 2015, Papachristou, Vallianos et al. 2018) has focused on wall-integrated active PCM systems. While these implementations do achieve load reductions, these studies show that integrating the PCM in the surface of a room has a detrimental effect on the controllability of the system, a necessary factor for maximum flexibility and peak load reduction.

This thesis presents a novel PCM-HX designed for installation in a ceiling plenum. This study explores the use of an active PCM-HX along with appropriate control strategies as an effective path to optimize the operation of a heating/cooling system. Such a dedicated active device offers the advantage of better controllability. Peak load reductions may also enable reducing the size of the HVAC unit at the design stage, thus leading to lower initial and operational costs.

The first part of this thesis investigates different design options for the integration of active PCM-HX, focusing on the optimization of the storage capacity and controllability. Several parameters are investigated towards achieving an optimal compromise between stored heat and a reasonable time needed to charge/discharge the PCM storage. These parameters include the

dimensions of the heat exchanger, the number of air channels and the airflow rate used to charge and discharge the PCM. The model used in this study for the specific heat of the PCM was validated experimentally; these results are also presented.

In the second part of the thesis, the integration of the aforementioned PCM-HX in an office zone is evaluated from the perspective of peak load reduction. This part examines the effect of using a linear ramp of room temperature setpoint transition on peak load reduction. Proportional-integral control (PI) is assumed in the local-loop control of room air temperature. The potential of combining diverse setpoint profiles with PCM designs with different number of air channels is also investigated.

Then, a simulation case study of an active thermal energy storage device with phase-change materials (PCM) for free-cooling is purposed. The effect of airflow rate on charging/discharging time is investigated. Then, different control strategies include discharging start times of the PCM-HX, discharge heat flow rate of the PCM-HX, and linear ramp of room temperature setpoint are also evaluated.

Finally the effect of the PCM-HX on energy flexibility in building is evaluated. The potential of shifting the energy use from high to low price periods is investigated. Time-of-Use Pricing (Ontario Hydro Rates) is used as an indicator of the price of electricity.

1.6. **Thesis outline**

Chapter 1: covers an introduction to the research topic including the motivation, background information, literature review, and of the work done and presented. This chapter focusing on the concept of building thermal energy storage systems with PCM and control strategies toward achieving better energy efficiency and energy flexibility. This chapter also contains the thesis outline.

Chapter 2: includes general concept and configuration of the presented PCM-HX device. It presents thermos-physical properties of the material and modes of operation of the PCM-HX. This section provides an overview of the numerical modeling of the PCM-HX along with the simplifications and some assumptions. The experiment set up and model validation of the PCM is presented at the end.

Chapter 3: presents evaluation of the design parameters, include PCM thickness (t_{PCM}), PCM-HX length (L_{PCM}), airflow rate through the channels, and the number of air channels.

Chapter 4: includes application of the PCM-HX integrated into the office zone under different control strategies. This is followed by exploring the sizing of the PCM-HX to achieve the optimal energy storage, peak demand reduction, and load shifting.

Chapter 5: investigates a free cooling system with active PCM heat exchanger (PCM-HX), in order to control the cooling load of an office space during summer.

Chapter 6: evaluates energy flexibility of a building with the PCM-HX for both summer and winter seasons.

Chapter 7: presents concluding remarks, a summary of the contributions and possible extensions to this research.

Under the work presented in this thesis, three paper has been produced, first one was presented at international conference of phase change materials (PCM-2018), the second one submitted to the IBPSA conference 2019, and the third one submitted to the journal of Energy and Building:

- Navid Morovat, Andreas K Athienitis. *Impact of building-integrated PCM on the indoor thermal environment and energy performance of an office zone*. 12th IIR Conference on Phase-Change Materials and Slurries for Refrigeration and Air Conditioning (PCM 2018). Orford (Québec), Canada, May 21- 23, 2018. (Accepted)

- Navid Morovat, Jose A. Candanedo, Andreas K Athienitis. *Performance Analysis and Control Strategies to Enhance Free Cooling with an Active PCM-Heat Exchanger*. 16th IBPSA International Conference & Exhibition Building Simulation (IBPSA 2019). Rome, Italy, Sep 2-4, 2019. (Submitted)

- Navid Morovat, Andreas K Athienitis, Jose A. Candanedo, Vasken Dermardiros. *Simulation and Performance Analysis of an Active PCM-Heat Exchanger Intended for Building Operation Optimization*. Energy and Buildings. (Submitted)

2. Chapter 2

This section introduce configuration of the PCM-HX device, thermos – physical properties of the PCM material, and modes of operation of the PCM-HX device during winter. This section also provides an overview of the numerical modeling of the PCM-HX along with the simplifications and some assumptions. The experiment set up and model validation of the PCM is presented at the end.

2.1. **Active PCM-HX: general concept**

The test building is 4 m wide, 4 m long and 3.2 m high, without internal partitions. The building, which is of lightweight construction, has a double glazing window in the middle of its south-facing façade (40% window-to-wall ratio (WWR)). The U-value of the window is 1.2 W/(m^2K) and its transmittance is 0.8. The bottom opaque section of the facade is 0.8 m high, matching the height of the work plane (Figure 2-1).

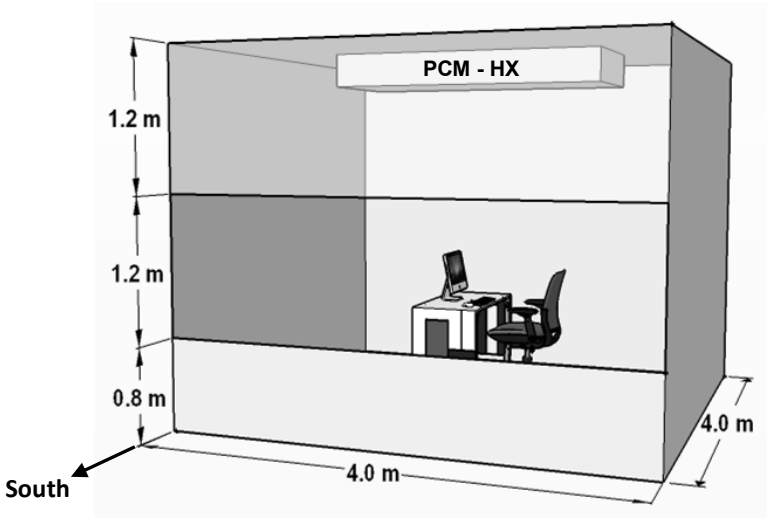

Figure 2-1. Schematic of the office zone with PCM-HX

2.2.**General concept**

The present study considers the integration of an actively charged PCM-HX for an office zone, as shown in Figures 2-2a and 2-2b. The PCM-HX system (located in this case in a ceiling plenum) is part of an insulated HVAC duct system. The PCM-HX system located in this case in a ceiling plenum because of availability of wasted space in the ceiling plenum (without taking useful space from the building). This place is also useful in terms of acoustic insulation between floors. An air-handling unit (AHU) with an electric coil, located just before the PCM-HX, is used to preheat the air entering the plenum. A circulation fan is used to drive air between the channels in order to charge/discharge the PCM.

During off-peak hours, the AHU is used to charge the PCM-HX by heating it. If heating is needed during on-peak hours: (a) the fan is turned on and (b) dampers between the room and the plenum are opened in order to discharge the PCM. The circulation fan is either ON or OFF (in other words, no operation at partial flowrates). If required, a baseboard heater can provide auxiliary heating directly to the room.

This PCM-HX configuration, which may be used as a practical retrofit measure, opens up the possibility of operating a lightweight building almost like a high-mass building, thus benefiting from the advantages commonly associated with materials with large thermal capacity (e.g., concrete).

The PCM-HX has the following modes of operation:

- **Charging mode:** both the AHU and the fan are turned on to charge the PCM (Figure 2-2a). The airflow passes through the PCM-HX, and is then recirculated back to the AHU. In this mode of operation, dampers are closed and there is no exchange between the plenum and the room air.
- **Discharging mode:** the AHU is turned off, but the circulation fan is turned on to discharge the PCM (Figure 2-2b). This mode of operation opens dampers that connect the plenum to the room air. Therefore, the discharge mode enables full air exchange with the room during peak load hours.
- **Standby mode:** both the fan and the AHU are off and the dampers are closed. In this mode of operation, there is no exchange between the plenum and the room air.

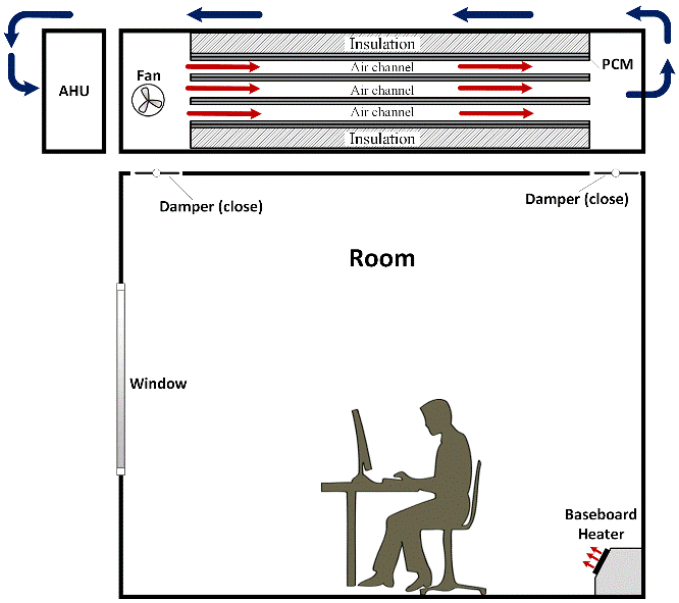

(a)

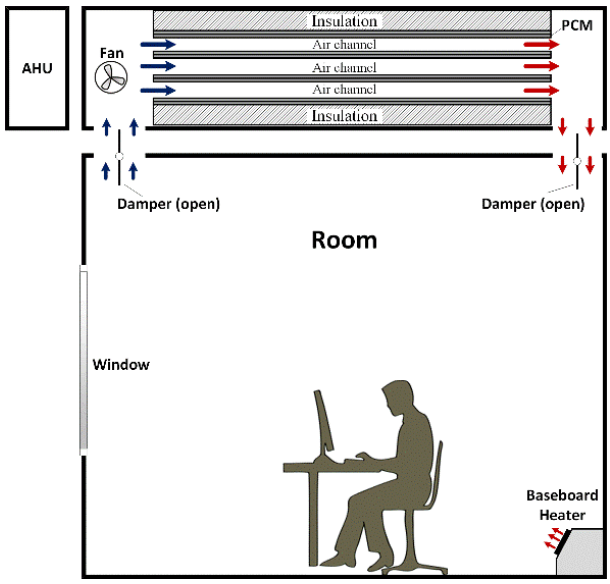

(b)

Figure 2-2. PCM-HX in isolated ceiling plenum (note: drawing not at scale). (a) Charging mode (during day), (b) Discharging mode (during night)

Such an active configuration, first described in an earlier study (Morovat and Athienitis 2018), provides more flexibility and controllability in terms of charging and discharging temperatures as compared to a conventional wall-integrated PCM system.

2.3. **Configuration of PCM-air heat exchanger (PCM-HX)**

Figure 2-3 presents a schematic of the proposed PCM-HX. This device consists of an arrangement of PCM panels that allows an airflow to pass between them. The length, width and thickness of each PCM panel are denoted by L_{PCM}, W_{PCM} and t_{PCM} respectively (standard measures given by the manufacturer are L_{PCM} = 1.2 m, W_{PCM} = 1.0 m and t_{PCM} = 5.2 mm). Several PCM panels may be installed "in series" in the PCM-HX; e.g., if n PCM panels are used then: $L_{HX} = n \times L_{PCM}$. For example, Figure 2-3 shows two panels connected in series, with a total length ($L_{HX} = 2L_{PCM}$). The simplicity of the proposed geometry makes this structure more adaptable to different configurations.

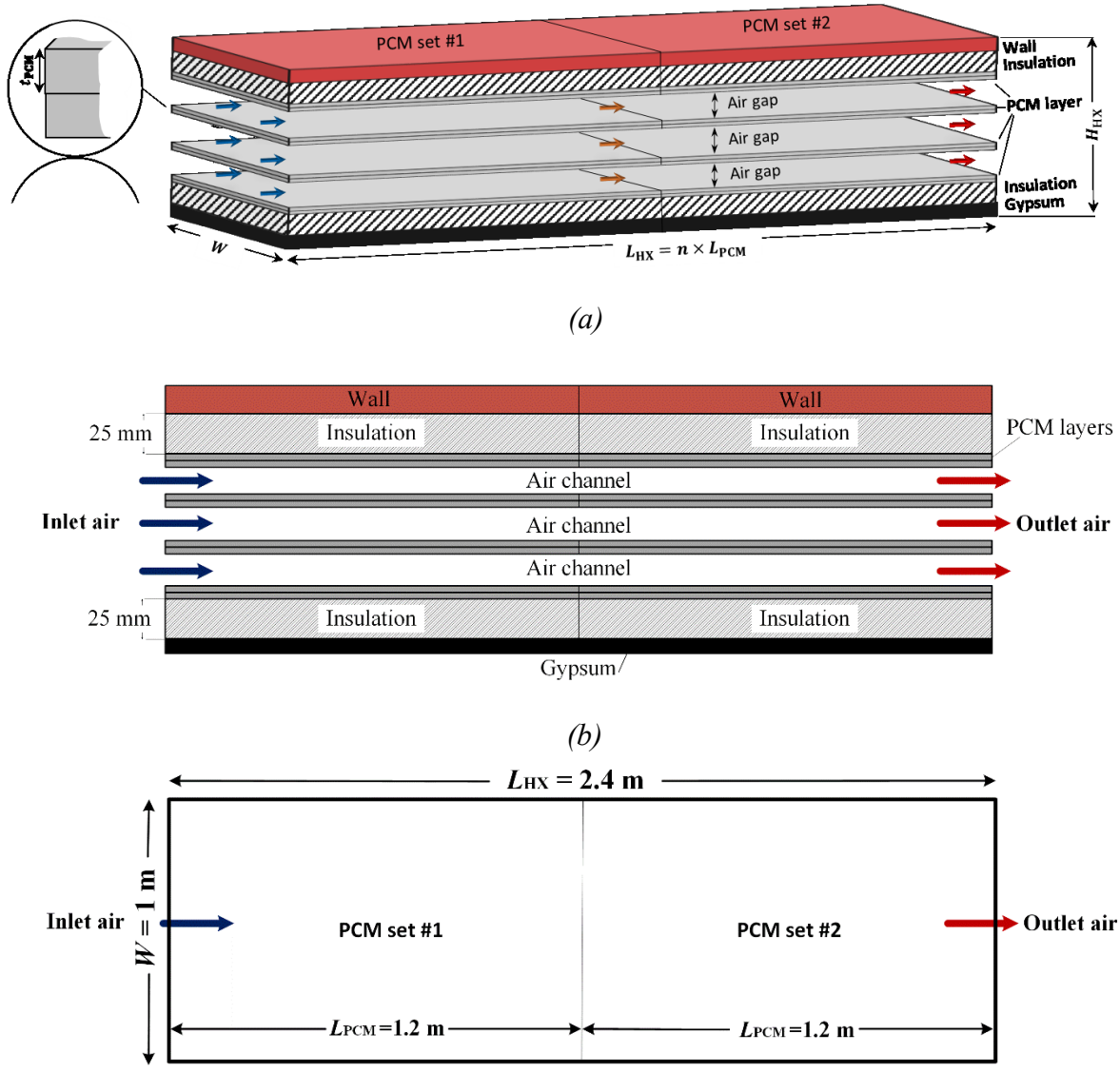

Figure 2-3. Schematic of PCM-HX. (a) Isometric view, (b) side view, and (c) top view (example with two PCM panels in series)

The PCM used in this paper is DuPont Energain^{TM}, which consists of a paraffin wax (60% wt) suspended in an ethylene-based polymer (Dermardiros 2015). Table 2-1 provides an overview of thermo-physical properties of the PCM used in the present paper. In a mechanically conditioned space, the best performance is achieved when PCM melting temperature is around the setpoint temperatures of the room (Fleischer 2015, Heier, Bales et al. 2015, Guarino, Athienitis et al. 2017).

In this thesis, PCM with melting temperature of 22.3 ºC and freezing temperature of 17.8 °C is used which makes it suitable for the heating and cooling season. These temperatures corresponds to indoor temperatures common in buildings.

Table 2-1. Properties of PCM used (Dermardiros 2015)

Element	Quantity
Thickness (base case)	5.2 mm
Density	850 kg/m^3
Average Specific Heat	3500 $kJ/kg \cdot$ K
Peak Melting Temperature	22.3 ℃
Latent Heat of Fusion	70000 J$/kg$
Peak Freezing Temperature	17.8 ℃
Conductivity, solid	0.22 W$/m \cdot$ K
Conductivity, liquid	0.18 W$/m \cdot$ K

2.4.**Modeling approach and Experimental validation**

An explicit finite difference scheme, implemented in Python 3.6, is used to numerically solve the heat transfer equations corresponding to the heat transfer phenomena in the office. Hed et al. (Hed and Bellander 2006) presented a similar method to simulate a PCM air heat exchanger: they found the effect of different shapes of specific heat curves –as a function of temperature– on the power of a PCM heat exchanger. In the present study, an enthalpy-temperature function for the PCM accounts for enthalpy changes during the phase change. This function is used to estimate an equivalent specific heat at each time step, which is then used in the finite difference equations for PCM.

2.5. **Governing equations**

Heat conduction within the heat storage is governed by Fourier's Law of heat conduction. Energy conservation equation is presented in equation 3 (Dolado, Lázaro et al. 2012):

$$\rho \frac{\partial h}{\partial t} + \nabla(-k(T) \cdot \nabla T) = 0 \tag{3}$$

In PCMs specific heat of the material vary with temperature, therefore, a finite difference approach is necessary. Equation 4 is a finite-difference formulation of the heat balance equation.

$$\sum_{J} \left[U_{ij}^{t}(T_j^t - T_i^t)\right] + \sum_{k} \left[U_{ik}^{t}(T_k^t - T_i^t)\right] - \frac{C(T)_i}{\Delta t}\left(T_i^{t+1} - T_i^t\right) + \dot{Q}_i^t = 0 \tag{4}$$

where

- U_{ij}: Conductance between nodes i and j equal to kA/dx for conductance, $h_{conv}A$ for convection and $h_{rad}A$ for radiation, W/K.
- U_{ik}: Conductance between nodes i and k where node k has a defined or known temperature (boundary condition), W/K.
- $C(T)_i$: Capacitance of node i equal to $\rho C_{\mathrm{p}}(T)Adx$, J/K
- $\dot{Q}$: Heat flow into the node, W
- Δt: Time step, s.

The equations in matrix form is:

$$\begin{Bmatrix} T_1 \\ \vdots \\ T_N \end{Bmatrix}^{t+1} = \begin{Bmatrix} \frac{\Delta t}{C_1} \\ \vdots \\ \frac{\Delta t}{C_N} \end{Bmatrix} \odot \left(\begin{bmatrix} -\sum_j^N U_{1j} - \sum_k^M U_{1k} + \frac{C_1}{\Delta t} & U_{12} & \dots & U_{1N} \\ \vdots & \vdots & \ddots & \vdots \\ U_{N1} & U_{N2} & \dots & -\sum_j^N U_{Nj} - \sum_k^M U_{Nk} + \frac{C_N}{\Delta t} \end{bmatrix} \begin{Bmatrix} T_1 \\ \vdots \\ T_N \end{Bmatrix}^t + \begin{Bmatrix} \dot{Q}_1 + \sum_k^M (U_{1kk} T_{kk}) \\ \vdots \\ \dot{Q}_N + \sum_k^M (U_{Nkk} T_{kk}) \end{Bmatrix} \right) \tag{5}$$

where,

- $\odot$: Is an element-wise multiplication operator,
- N: Is the number of nodes, and,
- M: Is the number of nodes with known temperatures.

To assure numerical stability in the solution, the time step must be chosen according to the stability criterion defined in equation 6:

$$\Delta t \leq \frac{\rho \cdot C_p(T) \cdot \Delta x^2}{2k} \tag{6}$$

2.6. **Modeling of specific heat within the PCM**

A continuous curve based on a skewed normal distribution requiring five parameters is used (Equation 7) to obtain the effective heat capacity of the PCM as a function of temperature (Dermardiros 2015). The curve is applicable to PCMs with limited sub-cooling, such as organic materials (Zalba, Marın et al. 2003). It offers a simplified method to input characterization data and improves simulation time.

$$C_{\mathrm{p}}(T) = \Delta h_{\mathrm{PCM}} \cdot \frac{1}{\sqrt{2\pi}} \cdot \exp\left(\frac{-(T - T_{\mathrm{c}})^2}{2 \cdot \omega^2}\right) \cdot \left[1 + erf\left(\frac{skew \cdot (T - T_{\mathrm{c}})}{\sqrt{2} \cdot \omega}\right)\right] + C_{\mathrm{p.average}} \tag{7}$$

where

- h_{PCM}, enthalpy of fusion, kJ/kg;
- T_{C}, approximate temperature of peak phase change, ℃;
- ω, temperature range of phase change, ℃;
- $skew$, skewness factor, ℃;
- C_{p}, average, average specific heat of PCM in the sensible range, $kJ/kg \cdot \mathrm{K}$;

The error function is Eq.8:

$$erf = \frac{2}{\sqrt{\pi}} \int_0^t \exp(-t^2)\, dt \quad (8)$$

Table 2-2 presents the specific heat equation values (DuPont -2019):

Table 2-2. Specific heat equation values for the PCM (DuPont - 2019)

Parameters	Melting	Freezing
$\Delta h_{\mathrm{PCM}}, kj/kg$	13100	12600
T_{c}, ℃	23.6	20.8
ω, ℃	4.5	4.7
Skew, ℃	-10	-4
$C_{\mathrm{p,average}}$, $kJ/kg \cdot \mathrm{K}$	3500	3500

This equivalent specific heat is then updated and used as input into finite difference model.

2.7. **Air control volume**

Figure 2-4 presents control volume of the air channel. For the air channel control volume, it is assumed that the temperature of the PCM surfaces are uniform within control volume.

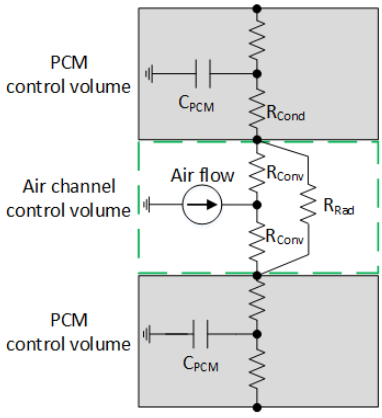

Figure 2-4. Air channel control volume

Equation 9 is the air control volume differential equation.

$$\dot{m} \cdot C_{\mathrm{p}} \cdot dT_{\mathrm{air}} = depth \cdot dy \cdot \left(h_{\mathrm{conv.front}} \cdot (T_{\mathrm{front}} - T_{\mathrm{air}}) + h_{\mathrm{conv.back}} \cdot (T_{\mathrm{back}} - T_{\mathrm{air}})\right) \quad (9)$$

Equation 10 is solved for the outlet air temperature to calculate the equivalent heat source at the air channel control volume (Equation 10).

$$T_{\text{air,outlet}} = T_{\text{air.inlet}} \cdot \exp\left(\frac{-h_{\text{conv}} \cdot A_{\text{PCM}}}{\dot{m}_{\text{air}} \cdot C_{\text{p.air}}}\right) + T_{\text{surface}}\left[1 - \exp\left(\frac{-h_{\text{conv}} \cdot A_{\text{PCM}}}{\dot{m}_{\text{air}} \cdot C_{\text{p.air}}}\right)\right] \quad (10)$$

$$\dot{Q}^{t}_{\text{PCM}} = \dot{m}_{\text{air}} \cdot C_{\text{p.air}} \cdot \left(T^{t}_{\text{air.outlet}} - T^{t}_{\text{air.inlet}}\right) \quad (11)$$

Equation 12 calculates the heat provided by the baseboard heater with proportional-integral control (PI controller) at each time step.

$$\dot{Q}^{t}_{\text{heater}} = k_{\text{p}} \cdot \left(T^{t}_{\text{setpoint}} - T^{t}_{\text{room.air}}\right) + k_{\text{i}} \int \left(T^{t}_{\text{setpoint}} - T^{t}_{\text{room.air}}\right) dt \quad (12)$$

where:

- k_{p}, proportional gain of the controller, W/K
- k_{i}, Integral gain of the controller, $\text{W/K} \cdot \text{s}$

Equations 3 through 7 were solved through an explicit finite difference formulation to calculate the total heat provided at the room air node. Two heat sources are applied at the room air node: one from the electric heater and the other from an equivalent source from the energy released from the PCM-HX.

2.8. **Convection heat transfer coefficient**

The convective heat transfer coefficient within the air channel depends on diverse factors: geometry, airflow rate, fluid and surface temperatures, etc. (Hed and Bellander 2006). Experimental results show that the corrected Martinelli equation (Eq.13) is appropriate for studying active thermal energy storage system with phase change materials with airflow in a cavity (Dermardiros and Athienitis 2015).

$$\mathrm{Nu}_{\mathrm{Martinelli}} = \frac{\mathrm{RePr}\sqrt{f/2}}{\left(\frac{T_\mathrm{w} - T_\mathrm{b}}{T_\mathrm{w} - T_\mathrm{p}} \cdot 5 \cdot (\mathrm{Pr} + \ln(1 + 5\mathrm{Pr}) + 0.5 N_{\mathrm{DR}} ln\left(\frac{\mathrm{Re}}{60}\sqrt{\frac{f}{2}}\right)\right)} \tag{13}$$

$$h_{\mathrm{conv}} = \frac{\mathrm{Nu} \cdot k_{\mathrm{air}}}{L} \tag{14}$$

2.9. **Experimental setup**

The experiments were conducted at the Paul Fazio Solar Simulator Environmental Chamber (SSEC) Research Laboratory (Concordia University, Montréal (Dermardiros 2015)). This experimental facility allows accurate and repeatable testing of advanced building enclosures under a wide range of conditions with fully programmable temperature, humidity, and pressurization. The temperature inside the SSEC can change in a range from –40°C to +50°C. The experiment is used to validate the numerical model of the PCM-HX with one air channel. The experimental test room has 5 layers of PCM panels integrated into the interior surface of the back wall of the room and located inside the Environmental Chamber. There is a 30 mm air channel between the 2nd and 3rd layers of the PCM.

Figure 2-4 provides schematic of the experimental setup includes environmental chamber and wall integrated PCM test room. The test room is 3 m wide, 1.5 m long, and 2.7 m high. A circulation fan is used to provide an air speed of around 2 m/s through air channel. A small auxiliary baseboard heater with capacity of 984 W is used to provide heat into the test room. The PCM used in this experiment has the same thermos-physical properties of the one used in the simulation. Thermo-physical properties of the PCM is presented in Table 1 (DuPont 2/15/2019).

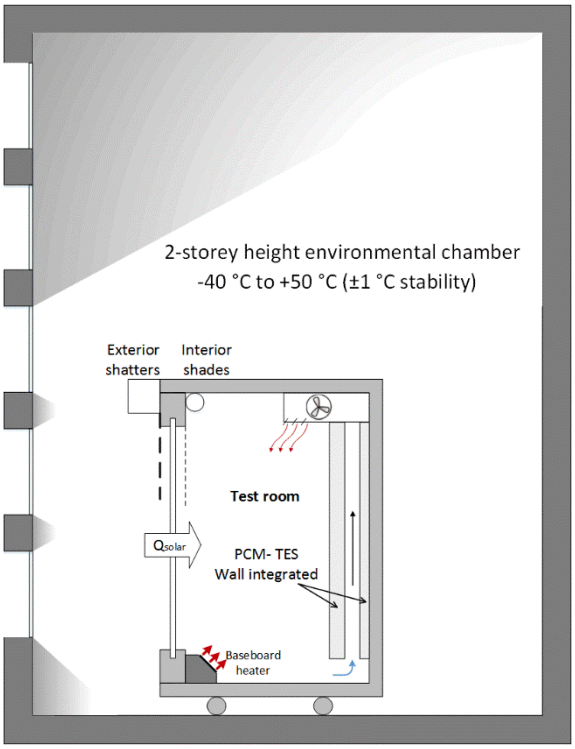

Figure 2-5. Schematic of the environmental chamber with wall integrated PCM test room. Adapted from Dermardiros (Dermardiros 2015)

Type T thermocouples (± 0.5 °C) are used to measure temperature in the PCM-TES. Environmental chamber provides warm/cool air through the PCM-TES. For charging the PCM, hot air stream enters by an inlet plenum of the PCM-TES and exits through an outlet plenum (Figure 2-5). The inlet and outlet plenum is installed in the test room to assure uniform airflow. At the beginning of the experiment, the PCM-TES is charged by supplying 28°C air at a rate of 400 kg/s (1.3 m/s average speed) until steady state is attained. This process is run twice to verify repeatability. The flow rate was chosen since it would provide a good convection heat transfer rate with lower pressure losses. The temperatures are read every 30 seconds and the average is recorded minutely. The experiments investigated the charge/discharge rate of the PCM under a temperature range of 16°C to 25°C in the test room. Details of the experimental setup is presented by (Dermardiros 2015).

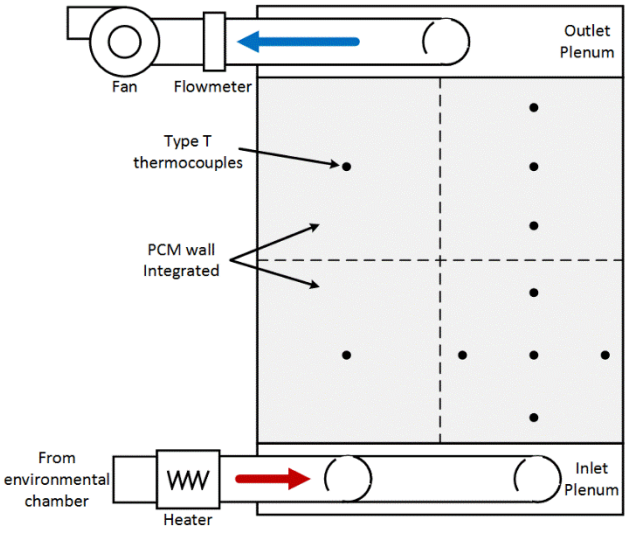

Figure 2-6. Schematic of the PCM wall integrated experiment. Adapted from Dermardiros (Dermardiros 2015)

2.10. **Experimental validation of the numerical simulation**

The current study shows how an explicit finite difference method with an enthalpy-temperature function for the PCM can be used as an effective tool in the design and implementation of the rule based control strategies in a test room with PCM-HX. Figure 2-6 and 2-7, presents a comparison between results of the numerical simulation in this thesis and corresponding experimental data (Dermardiros 2015), and their coefficient of variation of the root mean square error (CV-RSME). In this regard, the air outlet temperature (Figure 2-6) and energy transferred by the PCM-HX (Figure 2-7) is investigated. It was found that the PCM model can accurately predict the energy transferred by the PCM and the room temperature profile (CV-RSME $\leq$ 5%). While this experimental configuration is different from the proposed PCM-HX device, these results illustrate the validity of the PCM enthalpy model.

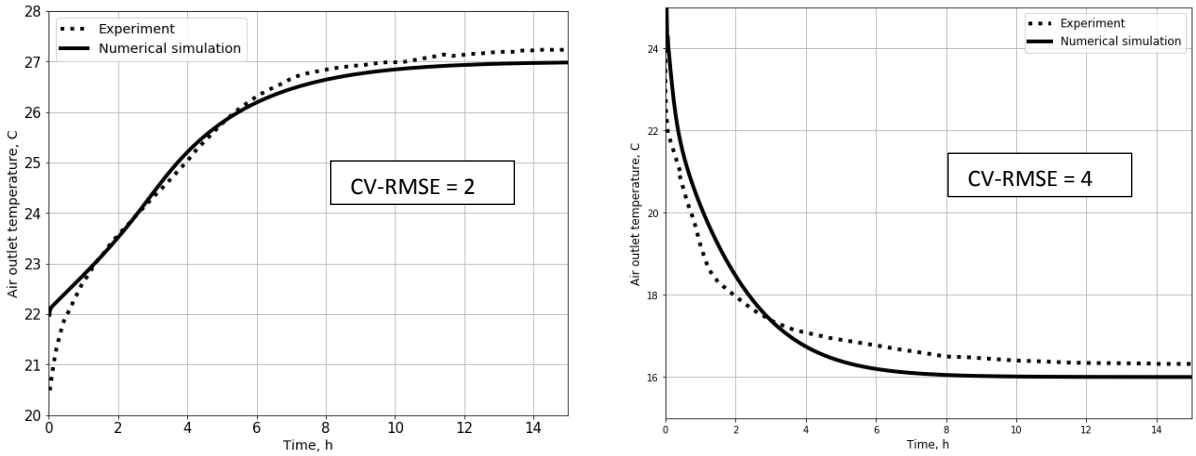

(a) **(b)**

Figure 2-7. Numerical simulation and experiment results for air outlet temperature: (a) Charging mode, (b) Discharging mode

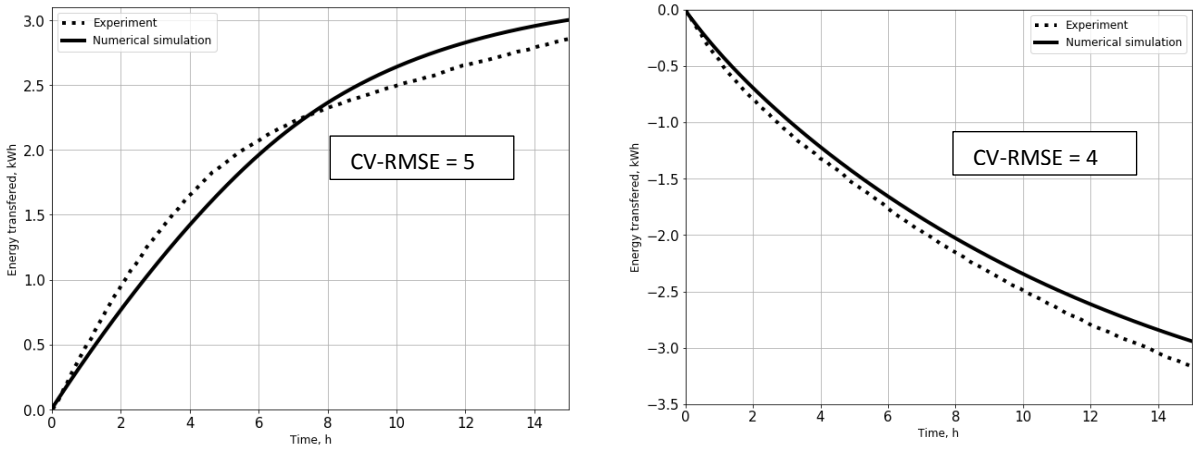

(a) **(b)**

Figure 2-8. Numerical simulation and experiment results for energy transferred of the PCM-HX: (a) Charging mode, (b) Discharging mode

2.11. **Conclusion**

This chapter presented general concept and configuration of the presented PCM-HX device. It provided an overview on the thermos-physical properties of the material and modes of operation of the PCM-HX. It also presented the numerical modeling of the PCM-HX along with the simplifications and some assumptions. The experiment set up and model validation of the PCM was provided at the end. It was found that the model of the PCM can accurately predict (CV- RSME $\leq$ 5 %) energy transferred and air outlet temperature from the PCM-HX.

3. Chapter 3

3.1. Design analysis

This chapter involves evaluation of the design parameters, which include PCM thickness (t_{PCM}), PCM-HX length (L_{PCM}), airflow rate through the channels, and the number of air channels. One parameter was fixed: the number of PCM layers, which was kept constant at eight (8).

3.2. Parameters investigated

The PCM-HX system is studied by varying the dimensions of the PCM and air channel, with different lengths (1.2, 2.4 and 3.6 m, corresponding to 1, 2 or 3 PCM panels in series). The inlet airflow rate was varied between 200 kg/h and 500 kg/h. Turbulent flow in the air domain was assumed ($3060 < Re < 7650$). Table 3-1 provides an overview of the values of all parameters investigated in this study.

Table 3-1. List of varied parameters

Case	Mass flow rate (kg/h)	Volume flow rate (L/s)	Average velocity (m/s)	PCM layer thickness (mm)	Air channel height (mm)	PCM-HX length (m)	Re number	Internal Convection Coefficient ($\mathrm{W}/m^2 \cdot \mathrm{K}$)
Effect of airflow	200	47.48	1.56	5.20	30.00	1.20	3060.00	9.62
	300	71.22	2.34	5.20	30.00	1.20	4590.00	15.32
	400	94.96	3.12	5.20	30.00	1.20	6120.00	20.50
	500	118.70	3.91	5.20	30.00	1.20	7650.00	26.62
Effect of PCM layer thickness	200	47.48	1.56	3.00	30.00	1.20	3060.00	9.62
	200	47.48	1.56	5.20	30.00	1.20	3060.00	9.62
	200	47.48	1.56	7.00	30.00	1.20	3060.00	9.62
	200	47.48	1.56	10.00	30.00	1.20	3060.00	9.62
Effect of PCM-HX length	200	47.48	1.56	5.20	30.00	1.20	3060.00	9.62
	200	47.48	1.56	5.20	30.00	2.40	3060.00	9.62
	200	47.48	1.56	5.20	30.00	3.60	3060.00	9.62
	200	47.48	1.56	5.20	30.00	4.80	3060.00	9.62

Air was assumed to have constant density, thermal conductivity and specific heat, with values of 1.184 kg/m^3, 0.0255 W/ (m·K) and 1006 J/ (kg·K), respectively. For each parametric combination, a numerical experiment was carried out by turning on the fan at time t = 0, and making it run for a 24-h period, with a constant inlet temperature of 10 °C. The results of the simulations are presented below.

3.3.**Effect of airflow through air channels**

Airflow rates of 200, 300, 400 and 500 kg/h were investigated for a configuration with one air channel (Figure 3-1).

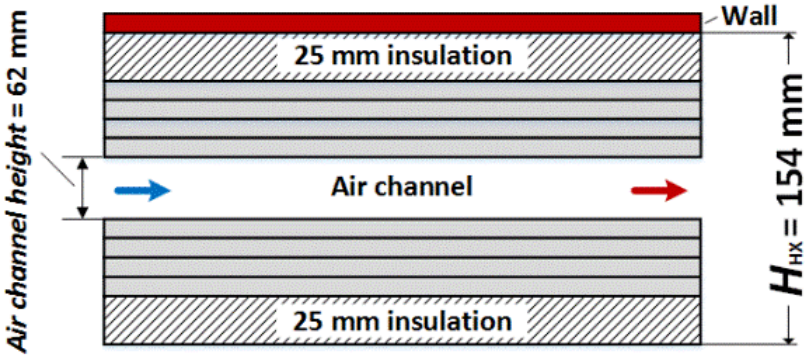

Figure 3-1. Schematic of PCM-HX with one air channel

Figure 3-2a and 3-2b provides the air outlet temperature and power delivered to the airstream by the PCM-HX for the different air flow rates, respectively.

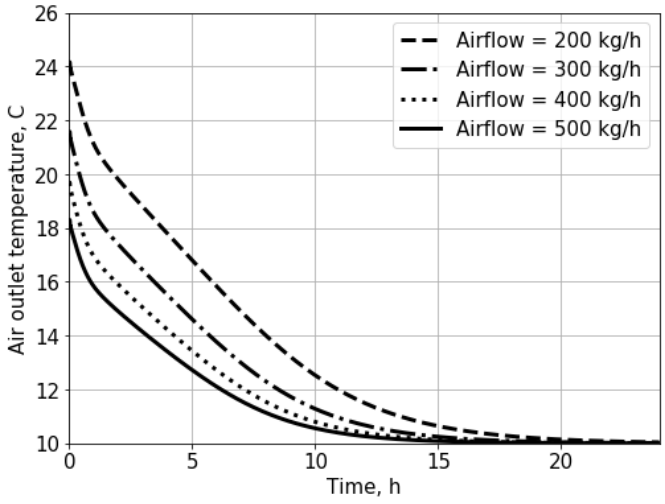

(a)

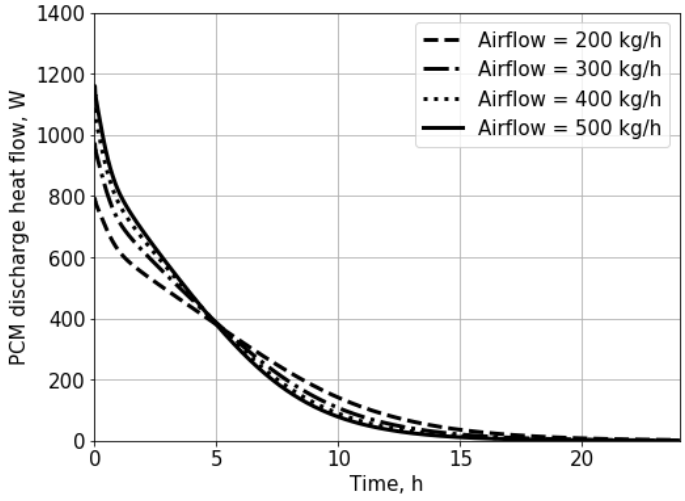

(b)

Figure 3-2. Effect of airflow on: (a) air outlet temperature, (b) PCM-HX power output of the PCM-HX

As expected, the air temperature difference between outlet and inlet decreases with the increase in airflow rate. The average temperature changes are 14 °C, 11 °C, 9 °C and 8 °C for air flow rates of 200, 300, 400 and 500 kg/h respectively.

At the beginning, high flow rates provide a higher power output (nearly 1200 W for 500 kg/h, versus 800 for 200 kg/h). However, low airflow rates discharge the PCM-HX more slowly. As a result, the average energy transfer over a 24 h period for the four air flow rates is approximately the same and amount to roughly 4.4 kWh. The amount of energy transferred was computed by using Equation 7.

3.4.**Effect of the thickness of PCM layers**

Another investigated parameter was the thickness of the PCM layers (see Table 3-1). Simulations were performed to determine the effect of the thickness of the PCM sheets in order to find the optimum PCM volume for the integration of the system in an office zone. Simulations

were done by testing several PCM-HX systems with PCM layers of various thicknesses (3, 5.2, 7, and 10 mm). Figure 3-3 presents the air outlet temperature and heating power delivered by the PCM-HX over a 24 h for different thicknesses.

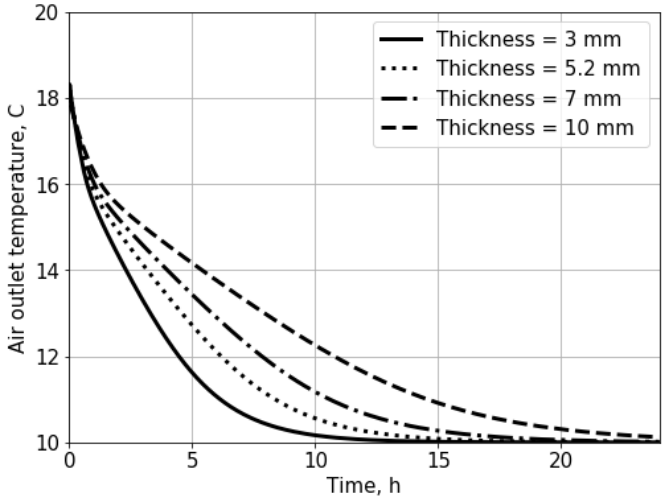

(a)

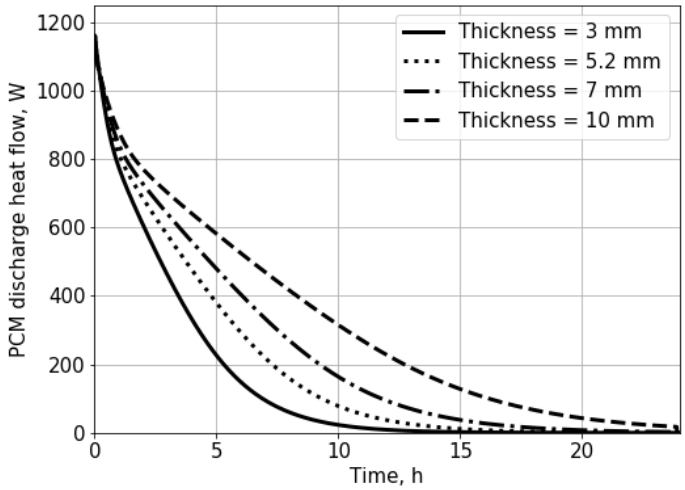

(b)

Figure 3-3. Effect of PCM layer thickness on : (a) air outlet temperature, (b) power output of the PCM-HX

Figures 3-3 show that the different configurations have a similar temperature decay profile. The slightly different temperature-profile is caused by the thicker volume of PCM layer used.

Increasing the thickness of the PCM layers results in higher outlet air temperature and higher PCM-HX output power. Thicker PCM sheets lead to a larger amount of energy stored; conversely, the larger thickness of PCM layer means longer times are needed to discharge them.

3.5.**Effect of length of the PCM-HX**

In this section, identical 1.20 m systems are placed "in series" (i.e., one after the other) to obtain devices with total lengths of 1.20, 2.40, 3.60 or 4.80 m. Figure 3-4 provide results regarding the effect of length of the PCM-HX on air outlet temperature and PCM-HX power.

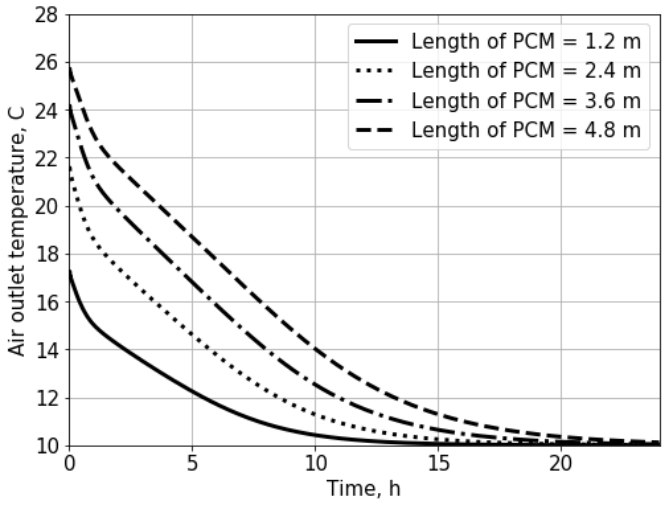

(a)

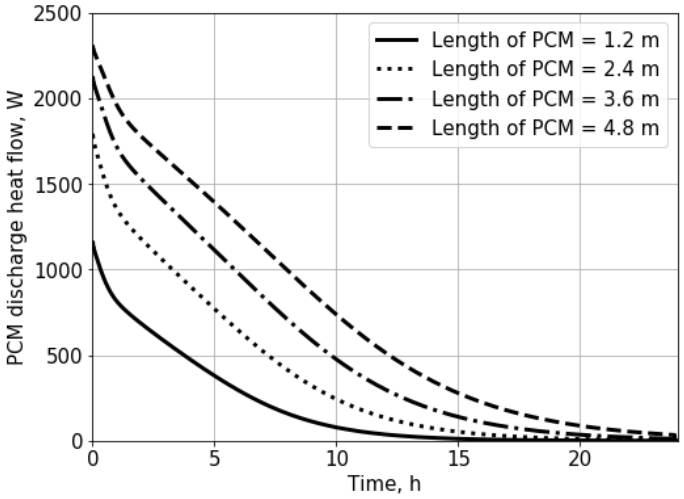

(b)

Figure 3-4. PCM HX length on: (a) air outlet temperature, (b) power output of the PCM-HX

Increasing the length of the PCM-HX leads to higher power output and also higher air outlet temperature, but charging/discharging the system takes more time. As expected, the difference between outlet and inlet air temperature increases with the increase in length of the PCM-HX. The difference between outlet and inlet air temperature are 7 °C, 12 °C, 14 °C and 16 °C for length of the PCM-HX equal to 1.2, 2.4, 3.6 and 4.8-m respectively. Longer PCM-HX devices imply higher pressure drops through the system, and consequently increasing fan power required. This another design factor that must be taken into account.

3.6.**Effect of number of air channels**

The number of air channels through the PCM layers was another parameter investigated. Figure 3-5 shows the different configurations of the PCM-HX consists of 8 PCM sheets with 1, 2, 3 or 6 air channels between layers studied in this paper.

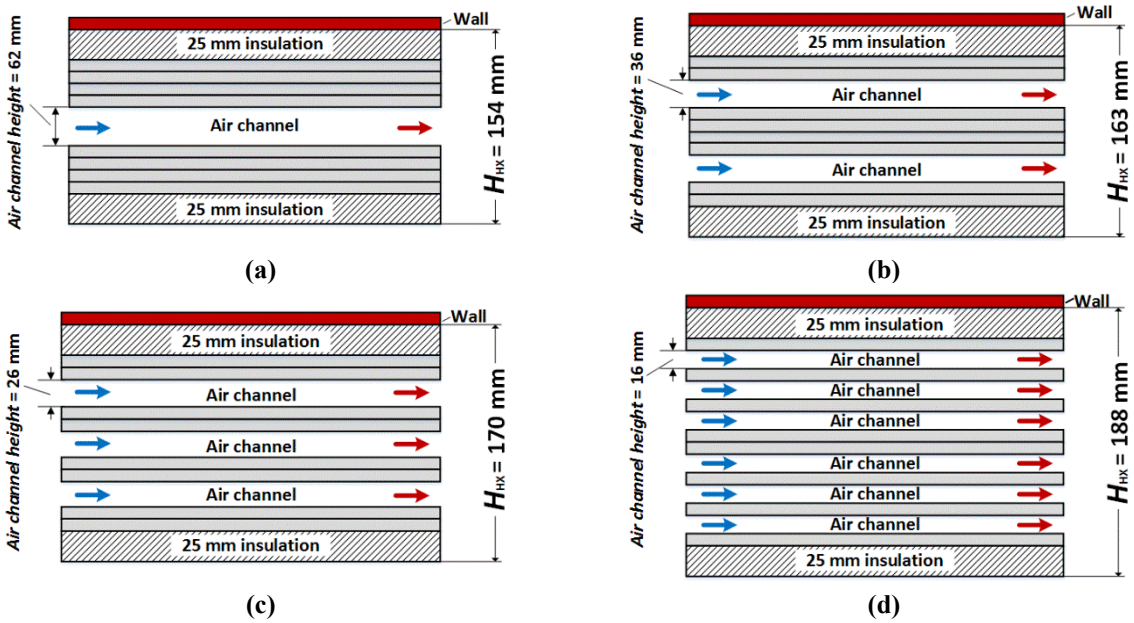

Figure 3-5. Schematic of PCM-HX with the different number of air channel: (a) one channel; (b) two channels; (c) three channels; (d) six channels.

The total mass flow rate considered is 600 kg/h (turbulent flow through air channels) for all cases with different number of air channels. For comparative purposes, the height of the channels and air velocity were chosen in order to maintain both a constant convective heat transfer coefficient and a constant total mass flow rate across the different systems (Dermardiros and Athienitis 2015). Accordingly, the inlet air velocity varies between 1.47 m/s and 2.23 m/s assuming turbulent flow in the air cavity. The smallest Reynolds number is 3040 for the 6-air channel configuration (slowest flow). Table 3-2 presents the value of the parameters for different number of the air channel.

Table 3-2. List of parameters for different number of air channel (Dermardiros and Athienitis 2015)

Number of channel	Total mass flow (kg/h)	Volume flow rate (L/s)	Mass flow $(kg/(s \cdot channel))$	Average velocity (m/s)	Air channel width (mm)	Convection Coefficient $(\mathrm{W}/m^2 \cdot \mathrm{K})$	Re number
1	600	142.40	0.17	2.23	62	18	17200
2	600	142.40	0.08	1.93	36	18	8830
3	600	142.40	0.06	1.75	26	18	5830
6	600	142.40	0.03	1.47	16	18	3040

The multi-channel active PCM-HX is analyzed comparatively using the thermal network model described in the section 2. Figure 3-6 presents the air outlet temperature of the PCM-HX, and PCM-HX power in 24 hours period for different number of air channels, respectively.

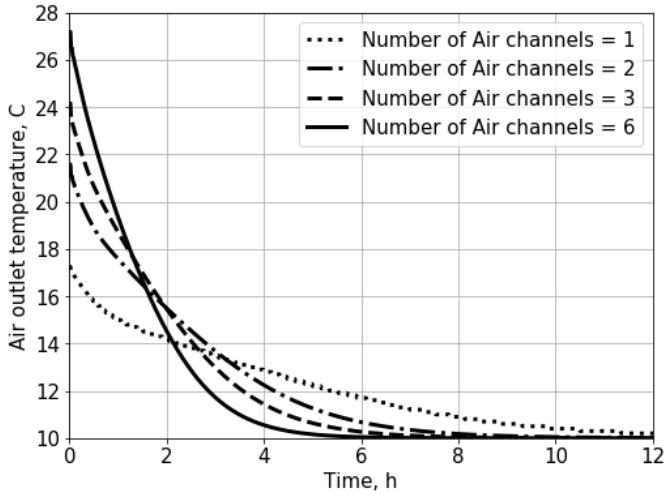

(a)

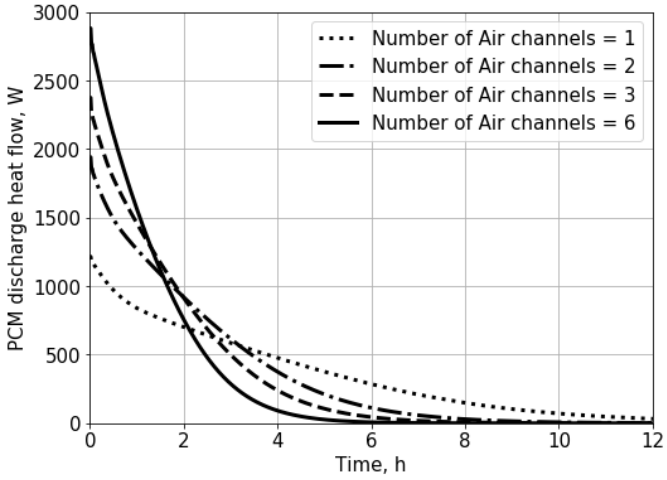

(b)

Figure 3-6. Effect of number of air channels on: (a) air outlet temperature, (b) power output of the PCM HX

Results show the charge/discharge time is inversely proportional to the number of channels. The single channel system would take more than 7 hours to charge, and would not be useful for fast peak reduction measures. A 6-channel PCM-HX system provides faster and more easily controllable storage of heat/cool. Table 3-3 provides summary of the results regarding energy per unit of volume of the PCM-HX (kWh/m^3), charging and discharging time (h) for different number of air channels.

Table 3-3. Energy density, charging and discharging time for different number of air channel

Number of channel	Energy per unit of volume of the PCM-HX (kWh/m^3)	Charging time (90%) (hr)	Discharging time (90%) (hr)
1 Channel	67.56	7.25	8.56
2 Channel	61.61	4.30	5.15
3 Channel	58.52	3.40	4.00
6 Channel	50.87	2.58	3.10

Based on the results presented in Table 3-3, although increasing the number of air channels leads to reducing energy per unit of volume of the PCM-HX, the charging and discharging times are shorter; in other words, “faster” (and arguably more controllable) PCM-HX devices. Increasing

the number of air channels from 1 to 6, reduced the energy per unit of volume of the PCM-HX by 25% while accelerating charging and discharging time by 64%.

3.7. **Energy density**

The optimal value of the PCM layer thickness is investigated in this section. Results show that an optimal value (in terms of energy density) exists. The objective is to find optimal design and operation needs to take into account the amount of stored heat of the PCM-HX.

Figure 3-7 presents the effect of the PCM layer thickness on the stored energy in PCM-HX for different number of air channels. Results show that for PCM layer thicknesses smaller than 15 mm the storage capacity is proportional to PCM volume and does not depend on the number of air channels. However, as the PCM layers become thicker, the maximum energy density also depends on the number of air channels. It was found that the maximum energy density was obtained for thicknesses ranging between 40 to 50 mm (Figure 3-7). For larger PCM layer thickness values (over 60 mm), charging/discharging rates decrease due to the relatively low thermal conductivity of the PCM panels. In addition, thicker panels result in increased thermal resistance within the PCM layers, and consequently lower energy density of the PCM-HX.

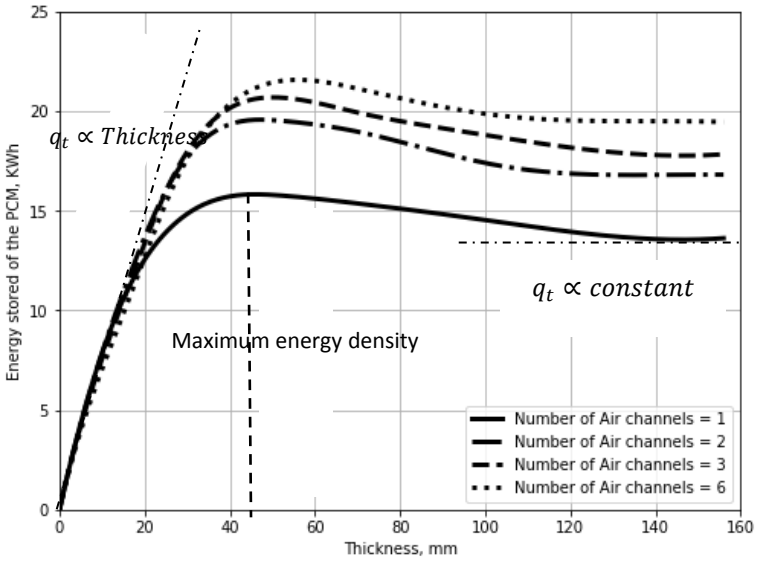

Figure 3-7. Effect of the PCM layer thickness on the stored energy in PCM-HX for different number of air channel

While PCM-HX with the PCM layer thickness of 40 to 50 mm has the maximum energy density, charging/discharging time is about 24 h. From a building operation standpoint, the charging/discharging time required is generally around 8 h or less, although in some applications (such as solar) one day discharge time could be of interest. Taking this into account, and considering the results provided in Table 5, a PCM layer thickness equal to 5.2 mm (used in this paper and is commercially available) is close to the "optimum thickness" when a discharge time of 8 hours or less is required.

3.8. **Conclusion**

This chapter investigated different design options of active PCM-HX charged and discharged with a controlled airflow in an office zone. The effect of thickness, length, number of the air channel, and airflow on the air temperature, and energy storage of the PCM-HX were evaluated. Results show that:

- Increasing the length of the PCM-HX leads to higher power output and also greater air-outlet temperature, but longer times are needed to charge/discharge the system. Results show, for building operation with charging/discharging time around 8 h or less, PCM-HX with 2.4 m length has a good thermal performance and controllability.
- A PCM layer thickness of approximately 5 mm (used in this study) has the best performance (charging/discharging time around 8 h or less), and is consequently the optimum thickness for the material properties considered.
- The difference between the outlet and inlet air temperature decreases with the increase in air stream rate, while the average energy transfers for different airflow rates are approximately the same. Therefore, in turbulence air stream through PCM-HX, lower the airflow rate leads to the better performance of the system (in terms of energy consumption and noise).
- Although increasing the number of air channels in PCM-HX causes reducing energy per unit of volume, the charging and discharging time decreases and lead to faster and more easily controllable PCM-HX. Increasing the number of air channel from 1 to 6, reduced energy per unit of volume by 25% while accelerate charging and discharging time by 64%.

4. Chapter 4

This chapter presents application of the PCM-HX integrated into the office zone under different control strategies targeting reductions in peak demand and HVAC system sizing during winter.

4.1. Control strategies

The appropriate application of control strategies in HVAC systems is a key factor to improve the energy efficiency (Tabares-Velasco, Christensen et al. 2012, Afroz, Shafiullah et al. 2017, Morovat and Athienitis 2018) and energy flexibility of buildings (Le Dréau and Heiselberg 2016, Jensen, Marszal-Pomianowska et al. 2017, Reynders, Lopes et al. 2018). Advanced control strategies for PCM, including predictive control have been investigated. For example, Barzin et al. (Barzin, Chen et al. 2016) studied the application of weather forecast to passive solar buildings with PCM; energy savings of about 31% were found.

The use of active thermal energy storage systems with PCM has not been widely adopted, mainly due to the lack of a proper integration into the building HVAC systems. In this regard, proper integration, including suitable control strategies, has a significant impact on the performance of the system. Also, if integrated with HVAC system design, the inclusion of the PCM-HX can be used to avoid the traditional oversizing of the HVAC equipment. Thus, both the operating and capital costs of the system can be effectively reduced.

The first part of the results presented in this paper discussed the amount of stored heat, the time needed to charge/discharge the PCM-HX storage and the overall energy density of the device. This section investigates the integration of the active PCM-HX within the HVAC system for peak load reduction. This study explores the sizing of the PCM-HX to achieve the optimal energy storage, peak demand reduction, and load shifting. This peak demand reduction may also enable smaller heating and cooling equipment and ducts, with a consequent reduction of system size and costs.

The following sections outline the results obtained from the application of the PCM-HX integrated into an office zone under two different scenarios. Firstly, the effect of discharging PCM-HX stored energy in a zone with step setpoints on the peak load has been studied. And then, the effect of using a linear ramp of room temperature setpoint on reducing peak load (with and without PCM-HX) is investigated.

4.2. **Design day conditions for control studies**

Weather conditions similar to a winter day in Montreal (i.e., a "Design Day") are selected as the simulation scenario, since the electrical power demand tends to peak under these conditions. Figure 4-1 presents the curves used to model outdoor temperature and solar flux on the south facade. In this simulation scenario, it is assumed that the outside temperature follows a perfect sine curve, fluctuating between -20 ºC and -10 ºC (thus having -15 ºC as a mean temperature, with an amplitude of 5 ºC). The peak temperature is reached at 3 pm. The time-varying solar flux is assumed to have a distribution representing an overcast cold day in February; this curve was obtained from a simulation carried out using EnergyPlus (Crawley, Lawrie et al. 2000) with a Montreal weather file.

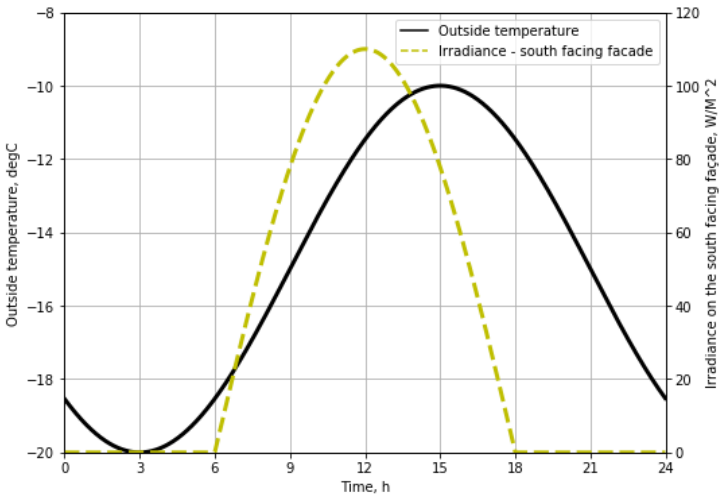

Figure 4-1. Outdoor temperature and solar flux on the south facade

4.3.**Numerical experiment**

It was assumed that the PCM-HX was well insulated on all sides (i.e., adiabatic conditions). The initial conditions of the experiment (just before $t = 0$) were the following:

- The initial temperature of the room was set at 18 °C everywhere.
- It was assumed that the PCM-HX was "fully charged": the material is fully melted and at a uniform temperature of 28 °C.
- Air from the room is circulated through the PCM-HX whenever heat extraction is required.

The simulation starts at t = 0 and runs for a period of 24 h using the weather conditions presented in Figure 4-1. The simulation time step was set to 60 seconds (it was previously determined that the critical time step for a finite difference formulation was 87 s). The heat provided by the baseboard heater was calculated by using a simple proportional-integral control. The actual controller in the experimental test room were used in the model. Proportional gain of the controller (k_P) is assumed to be twice the capacity of the electric baseboard heater per degree (e.g., if the baseboard capacity is 3000 W, k_P = 6000 W/K), and the k_i is considered to be 0.1 W/K·s

4.4. **Peak load shifting with PCM-HX**

Lowering the temperature setpoint at night is an effective way to reduce energy consumption (Manning, Swinton et al. 2005, Moon and Han 2011). In this regard, the setpoint during daytime (between 6:00 to 18:00) is 22°C for heating. During the nighttime (between 18:00 to 6:00), the set point is 18 °C for heating. In this paper, the energy released from the PCM-HX is primary heating system and an electric baseboard heater is an auxiliary system.

It should be taken into account that oversized systems cycle off before they completely heat or cool a zone. In addition, an undersized system runs constantly trying to heat the zone, but it cannot provide the required thermal comfort. Therefore, having an HVAC system properly sized that matches the demand can provide thermal comfort while reducing peak loads. With this in mind, a baseboard heating system with capacity of 1000 W is used. The charging mode of the PCM-HX device is from 0:00 to 6:00 (off-peak hours) and discharging mode is from 6:00 to 15:00 (on-peak hours). The application of the PCM-HX system toward achieving peak load shifting and peak load shaving has been investigated under these conditions.

Figure 4-2 shows thermostat set point and room air temperature with and without PCM-HX. As can be seen, the baseboard heater without a PCM-HX could not reach the required setpoint. Conversely, these results show that using PCM-HX keeps comfortable conditions, even with a small baseboard. Figure 4-3 presents a comparison of the results for the electric load (AHU coil + baseboard heater) with and without PCM-HX.

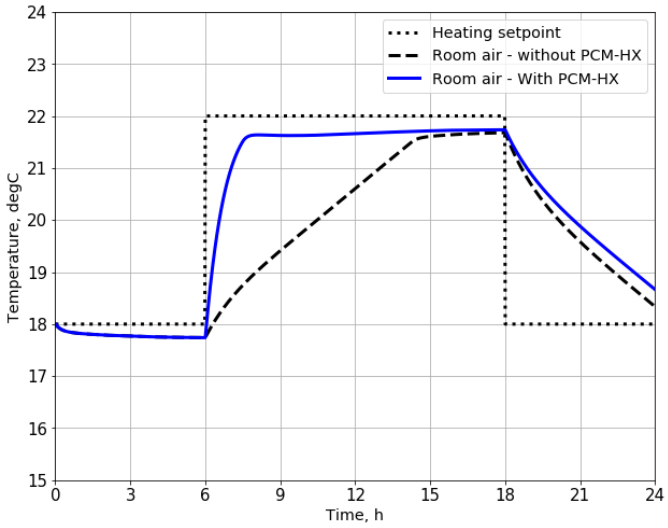

Figure 4-2. Temperature setpoint and room air temperature

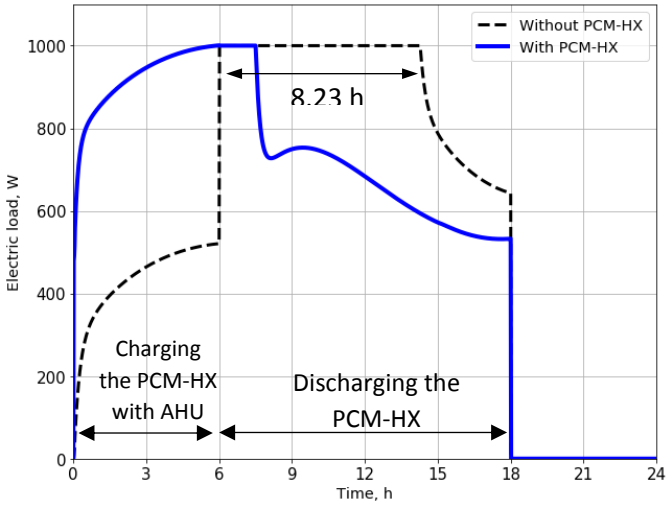

Figure 4-3. Heating load with and without PCM-HX

The results show that using PCM-HX could reduce peak load duration from 7 hr to 1 hr. Figure 4-3 shows that using PCM-HX shifts the peak load from on-peak hours to off peak hours and reduces the peak load *duration* by 86 %, therefore reduces mean power load during daytime (W) by 25% from 877 W to 665 W.

4.5. **Peak load reduction with PCM-HX and linear ramp of room temperature set point**

It is well known that a sudden setpoint transition –e.g. between a night setback and daytime setpoint– creates a spike in the peak demand. The effect of using ramps to transition between setpoints has been investigated by (Braun and Lee 2006, Lee and Braun 2008, Candanedo, Dehkordi et al. 2015), among others.

This section examines the effect of using two-hour linear ramp of room temperature set point on reducing peak load in a room equipped to PCM-HX with six air channels. In this case, a baseboard heater with capacity of 3000 W is used for better thermal comfort. The charging mode of the PCM-HX device is from 0:00 to 4:00, and discharging mode is from 04:00 to 15:00. Figure 4-4 presents thermostat set point with ramp and room air temperature. Figure 4-5 presents results regarding heating load required considering ramp in set point temperature with and without PCM-HX.

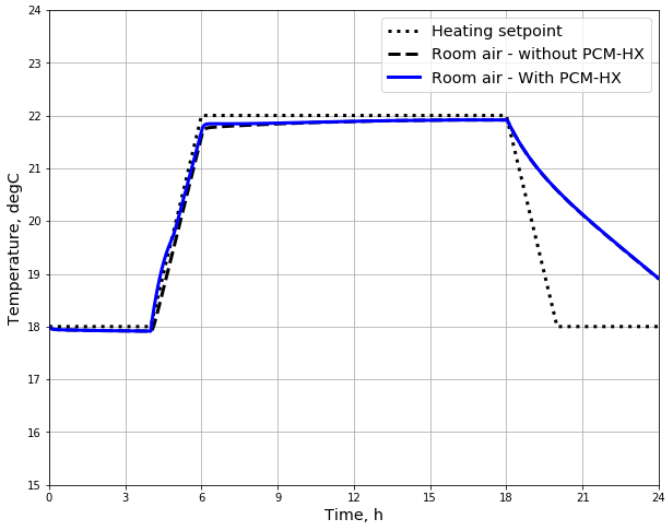

Figure 4-4. Temperature setpoint with ramp and room air temperature

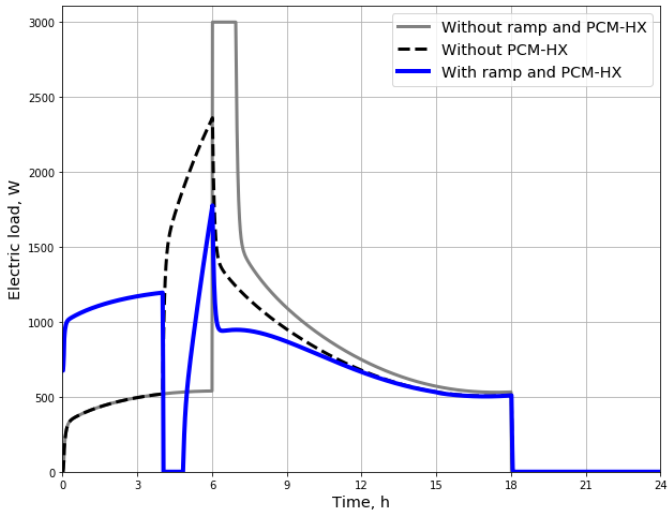

Figure 4-5. Heating load with and without PCM-HX – set point temperature with ramp

Results presented in Figure 17 show that a 2 hour ramp in temperature set point can reduce peak load by 31% from 3000 W to 2050 W. The combination of the 2 hours linear ramp and PCM-HX energy with six air channels provide 51% peak load reduction from 3000 W to 1467 W.

4.6. **Conclusions**

In this chapter, the integration of the proposed PCM-HX in an office zone was evaluated along with the effect of enhanced control strategies. The potential of using PCM-HX with different number of air channels together with linear ramps is investigated. The main results are:

- The combination of a small baseboard heater (1000 W), and PCM-HX with six air channels shifts the peak load from on-peak hours to off peak hours and reduces the peak load *duration* by 82 %, and 31% reduction in mean power load during daytime, relative to a reference case without the PCM-HX;
- For a larger baseboard heater (3000 W), the combination of the two-hours linear ramp of temperature setpoint and PCM-HX with six air channels provides 41% peak load reduction, and 22% reduction in mean power load during daytime, relative to a benchmark case without the PCM-HX;

Results shows that the use of active PCM-HX and appropriate control strategies could be an effective solution to have better energy flexibility in buildings, reduce the sizing of the HVAC unit at the design stage and to enhance energy cost reductions, thus possibly reducing both operation and initial capital costs.

5. Chapter 5

5.1. Free cooling

This section presents a simulation case study of the presented PCM-HX device for free-cooling purposes. First, the effect of airflow rate on charging/discharging time is investigated. Then, different control strategies targeting reductions in peak demand and HVAC system sizing are evaluated.

5.2. PCM for free cooling applications

Zhu, Ma et al. (2009) presented an overview of research conducted on PCMs concerning their dynamic characteristics and energy performance in buildings. This overview showed that there is particular interest of PCM applications in free cooling.

In passive applications, PCMs are integrated into the building envelopes to increase the effective thermal storage capacity in order to better energy saving and temperature regulation. The main problem with incorporating PCMs in the building envelope is the difficulty of exchanging a high rate of heat between the air and the PCM. Passive ways for cooling may also not be as effective in extreme climate conditions. This is mainly because of the outdoor ambient air temperature does

not decrease sufficiently at night. Stetiu and Feustel (1998) found that for climates with relatively high ambient temperatures (above 17 °C) during the night, it would be beneficial to force the supply air along the storage surfaces to facilitate good heat exchange.

5.3.**Free cooling**

Free cooling has been defined as "cool[ing] the building interior with or without minimum electricity usage" (Givoni 1984, Santamouris and Asimakopoulos 1996, Szokolay 2012).

In free cooling, a TES is used to store the "ambient cold" to be used later during hot daytime periods (Stritih 2003, Zalba, Marín et al. 2004). Thermal energy for free cooling can be stored by using: sensible heat storage, latent heat storage or the combination of both (Dincer and Rosen 2002, Sharma, Tyagi et al. 2009). In this application, Latent Heat Thermal Energy Storage (LHTES) by PCMs is often preferred over other storage techniques due to its high energy storage density and isothermal storage process (Waqas and Din 2013). Cool air during the night is used to solidify the PCM and the accumulated cooling capacity is then extracted when required. Given the large variety of available PCM materials with different thermal properties (such as latent heat storage capacities and phase change temperatures) they can be used in multiple applications. For free cooling systems, PCMs have to be selected so that the cooled air temperature is within the range of human comfort, a zone which can vary significantly according to a number of factor (Heier, Bales et al. 2015).

5.4.**Modes of operation in free cooling application**

In the present study, the integration of the active PCM-HX in an office zone for free cooling application is investigated (Figures 5-1a and 5-1b).

If cooling is needed during on-peak hours: the fan is turned on and dampers are opened, in order to discharge the PCM-HX. Note that in this concept no cooling coil is used to lower the temperature of the PCM-HX.

The following modes of operation are implemented for the PCM-HX:

- **Charging mode:** the circulation fan is turned on to bring outside air through PCM-HX during night to charge the PCM (Figure 5-1a). In this mode of operation, dampers are close and there is no exchange between the plenum and the room air.
- **Discharging mode**: In this mode, the dampers are opened and circulation fan is turned on during hot day to discharge the PCM (Figure 5-1b). Therefore, the discharge mode enables full air exchange with the room during peak load hours.
- **Standby mode**: the fan is off and dampers are closed. In this mode of operation, there is no exchange between the plenum and the room air or outside air.

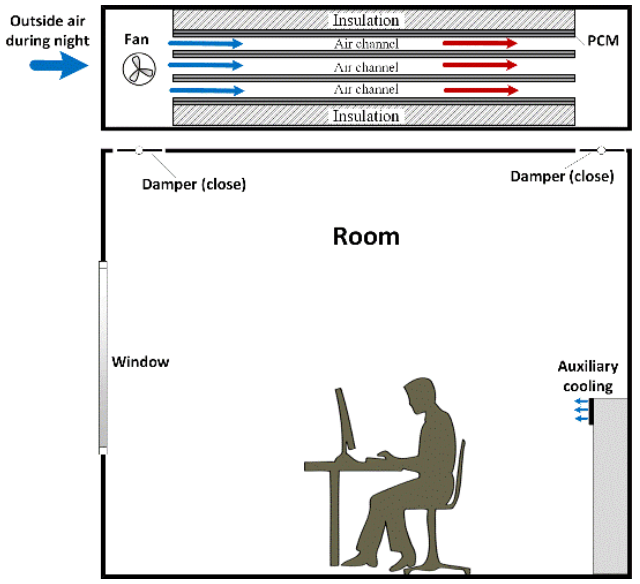

(a)

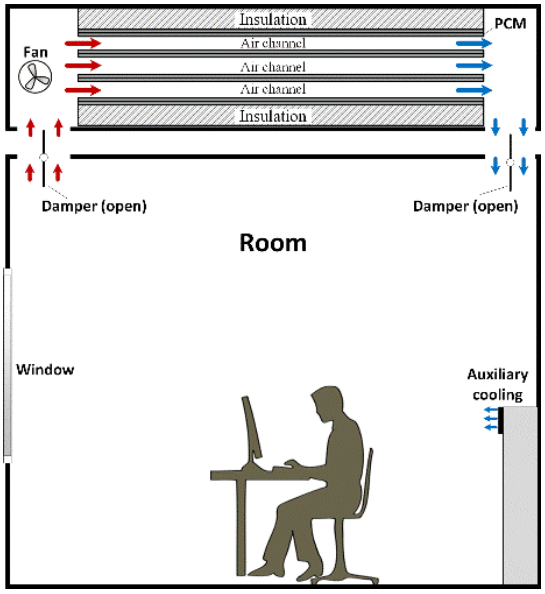

(b)

Figure 5-1. PCM-HX in isolated ceiling plenum (note: drawing not at scale). (a) PCM-HX in charging mode- during night, (b) PCM-HX in discharging mode – during day

The melting point of the PCM plays an important role in the design of the storage unit (Arkar, Vidrih et al. 2007). For free cooling applications, PCMs should be selected in such a way that the cooled air temperature of the PCM-HX be within the range of defined comfort levels (Stritih and Butala 2007, Butala and Stritih 2009) which is between 23 ºC and 27 ºC for summer season.

Therefore, for free cooling systems, the melting temperature of the PCM should be between 19 ºC and 24 ºC (Butala and Stritih 2009). In a mechanically conditioned space, the best performance is achieved when PCM melting temperature is around (±2 ºC) the setpoint temperatures of the room (Heier, Bales et al. 2015, Guarino, Athienitis et al. 2017).

In view of these considerations, a PCM with melting temperature of 22.3 ºC is used in this thesis. Such a material is suitable for the cooling season and is commercially available. In this paper, the PCM-HX system has 2.4 m length, (corresponding to two PCM panels in series), and the analysis is limited to eight sheets of PCM. Figure 5-2 provides a schematic of the PCM-HX with 6 air channels between layers.

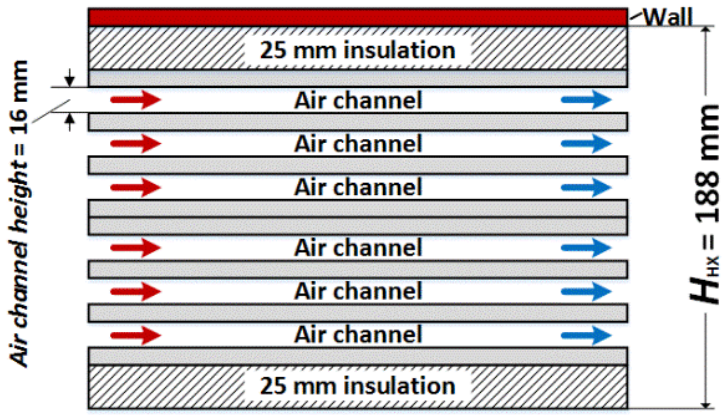

Figure 5-2. Schematic of PCM-HX with six air channels.

Results of this section are presented in two parts:

(a) Evaluation of the charging/discharging time of the PCM-HX.

(b) Application of the free cooling with PCM-HX under different control strategies toward reducing peak load reduction and energy use.

5.5.**Charging /discharging time**

A high temperature difference between PCM melting point and the incoming airflow facilitates freezing the PCM the charging process at night. If the temperature difference is small, high air flow rates are needed to solidify the PCM completely in the required period (Turnpenny, Etheridge et al. 2000, Yanbing, Yi et al. 2003, Zalba, Marín et al. 2004, Saman, Bruno et al. 2005)

In free cooling applications, the nighttime period that allows charging the PCM is rather short. Consequently, higher airflow rates can ensure the maximum charging of the PCM storage. For free cooling applications, it has been recommended that the charging process airflow rates be three to four times those used during discharge process (Arkar and Medved 2007, Arkar, Vidrih et al. 2007, Medved and Arkar 2008). Conversely, during the discharge process, lower flow rates are better than high flow rates to maintain the outlet air temperature within the defined comfort levels (Arkar, Vidrih et al. 2007).

In this regard, for PCM-HX with 6 air channels, the total mass flow rate considered is 600 kg/h in charging mode of operation (during night), and 250 kg/h in discharging mode (during hot day). The PCM-HX operates between 17 ºC (as an example of outdoor temperature at night) and 24 ºC (room temperature setpoint during day). Table 5-1 presents parameters for charging and discharging mode of operation.

Table 5-1. List of parameters in charging and discharging mode of operation

Parameter	Charging mode	Discharging mode
Total mass flow (kg/h)	600.0	250.0
Volume flow rate (*L*/*s*)	142.4	47.5
Average velocity (*m*/*s*)	1.5	0.5
Air channel width (*mm*)	16.0	16.0
Convection Coefficient ($W/m^2 \cdot K$)	18.0	15.0
Re number	3050.2	1270.9

Figures 5-3 and 5-4 present the air outlet temperature, and PCM-HX charge/discharge heat flow in 24 hours period, respectively.

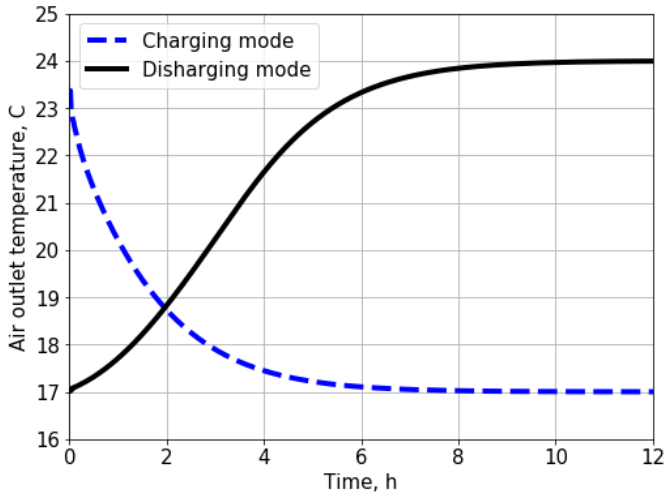

Figure 5-3. Air outlet temperature for charging/discharging PCM-HX

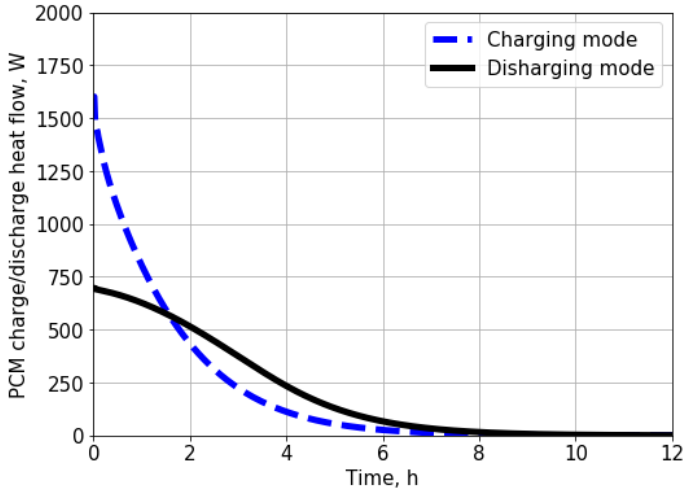

Figure 5-4. PCM-HX charge/discharge heat flow

It can be seen from Figures 5 and 6 charging time (90% of total) is around 4 h, while discharging (90% of total) time is around 6 h.

5.6.**Control strategies**

The following sections outline the results obtained from free cooling application of the PCM-HX under three different scenarios toward achieving peak load and energy consumption reduction.

- The effect of discharging PCM-HX stored energy in a zone with step setpoints.
- The effect of using a linear ramp of room temperature setpoint.
- The effect of discharging start time of the PCM-HX.

5.7.**Design day conditions for control studies**

Weather conditions is similar to a summer day (Design Day) in Montreal. Figure 5-5 presents the curves used to model outdoor temperature and solar flux on the south facade. In this simulation scenario, the outside temperature fluctuats between 15 ºC and 26 ºC (thus having 20.5 ºC as a mean

temperature and an amplitude of 5.5 ºC). The peak temperature is reached at 3 pm. The time-varying solar flux is assumed to have a profile representing a clear hot day in July. This curve was obtained from a simulation carried out using EnergyPlus (Crawley, Lawrie et al. 2000) with a Montreal weather file.

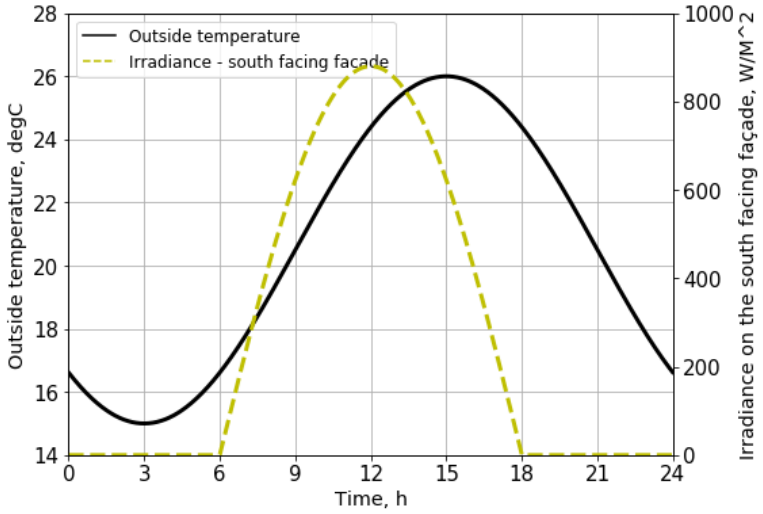

Figure 5-5. Outdoor temperature and solar flux on the south facade

5.8. **Numerical experiment for free cooling**

It was assumed that the PCM-HX was well insulated on all sides (i.e., adiabatic conditions). The initial conditions of the experiment (just before $t = 0$) were the following:

- The initial temperature of the room, at $t = 0$, was set at 26°C (setpoint temperature) everywhere.
- It was assumed that the PCM-HX was "fully charged": the material is fully solid and at a uniform temperature of 17 °C.
- Air from the room is circulated through the PCM-HX whenever heat extraction is required.

The simulation starts at $t = 0$ and runs for a period of 24 h using the weather conditions presented in Figure 5-5. A heat pump with COP = 3 is considered as the auxiliary cooling system. Capacity of the cooling system is assumed 3500W. The proportional gain of the controller (k_P) is 4000 W/ ºC and the integral gain of the controller (k_i) is 0.1 W/ºC·s.

5.9. **Effect of discharge heat flow rate of the PCM-HX**

The setpoint temperature during daytime (between 6:00 to 18:00) is assumed 24°C for cooling and during nighttime (between 18:00 to 6:00), the set point is 26 °C. The charging mode of the PCM-HX device is during nighttime and discharging mode is during daytime.

In this section, two scenarios regarding effect of heat flow rate of the PCM-HX on peak load reduction has been investigated:

(1) Scenario #1: PCM-HX with laminar air stream through the air channels: airflow rate is 250 kg/h (Re= 1270.9, air velocity = 0.5, and $h_c = 15$)

(2) Scenario #2: PCM-HX with turbulent air stream through the air channels: airflow rate is 600 kg/h (Re= 3050.2, air velocity = 1.5, and $h_c = 18$)

Figure 5-6 presents a comparison of the results for the electric load, and figure 5-7 shows temperature setpoint and room air temperature with and without PCM-HX.

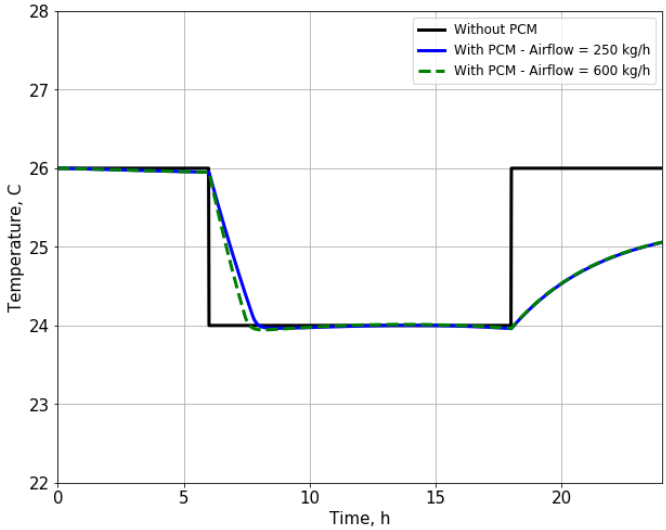

Figure 5-6. Temperature setpoint and room air temperature

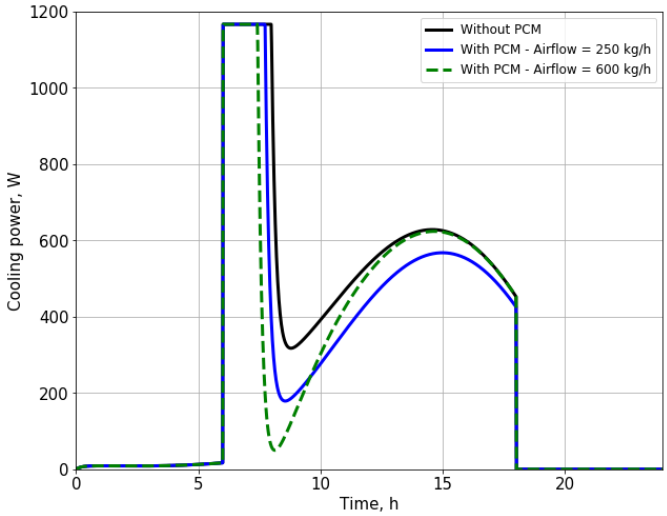

Figure 5-7. Auxiliary cooling power – different airflow through PCM-HX

The results show that the free cooling with PCM-HX could reduce energy consumption by 14% from 7.6 kWh to 6.55 kWh. In peak load perspective, higher the airflow rate, leads to faster discharge of the PCM-HX, without significant effect on peak load (around 1%). On the other hand, lower the airflow rate causes smooth reduction in energy consumption during all hours of the day, and peak load reduction as well. In this case, peak load during hot daytime (2:30 P.M) reduces by 4%.

5.10. **Effect of discharging start times of the PCM-HX**

In previous sections, it was found discharging PCM-HX from early morning (from 6:00 A.M) causes 8% peak load reduction.

In this section, three more scenarios has been investigated:

(1) Scenario #3: Two-hours linear ramp of temperature setpoint (from 4:00 to 6:00, and 18:00 to 20:00)

(2) Scenario #4: Discharging PCM-HX from 09:00 A.M.

(3) Scenario #5: Discharging PCM-HX from 13:00 P.M.

It should be taken into account that airflow rate trough air channels is assumed 600 kg/h, due to reducing in time of discharging PCM-HX. Figure 5-8 provides a comparison between results for different discharging start times of the PCM-HX, and Figure 5-9 presents Temperature setpoint and room air temperature with ramp.

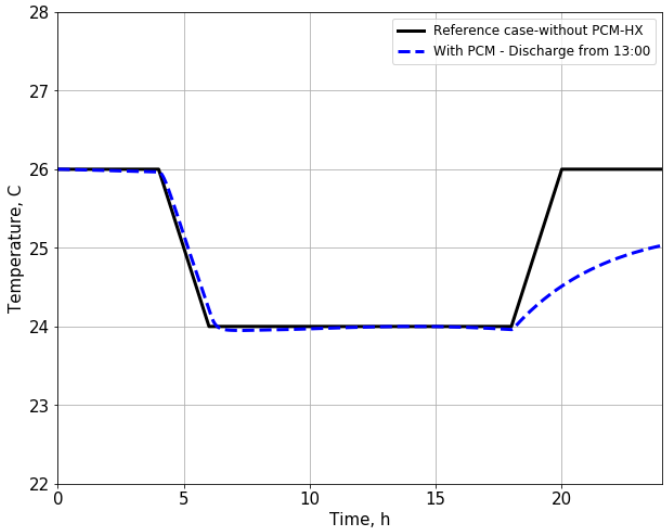

Figure 5-8. Temperature setpoint and room air temperature with ramp

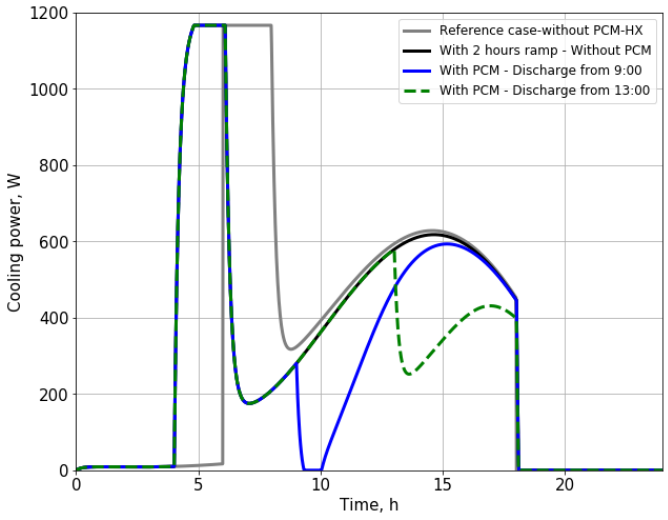

Figure 5-9. Auxiliary cooling power – different discharging start times of PCM-HX

It was found using two-hour linear ramp of room temperature set point could shift peak load in an effective manner. Results show, for the case with discharging start time from 09:00, cooling power fluctuation increases by 44 % compared to the reference case; while in the case with discharging start time from 13:00 cooling power fluctuation reduces by 24 % compared to the reference case.

The simulation studies in this study shows that airflow rate through air channels and discharging start times of the PCM-HX are two important factors toward achieving best performance of free cooling with PCM-HX. In a future work, the performance of the PCM-HX will be optimized for free-cooling applications by applying a model predictive control (MPC) method to determine optimal flow rates and discharging start times.

5.11. **Conclusion**

In this chapter, the integration of the proposed PCM-HX for free cooling in an office zone is evaluated along with the effect of enhanced control strategies. The potential of using PCM-HX with different number of air channels together with linear ramps is investigated. The main results are:

- The PCM-TES is charged (90% of its capacity) in 4 h and discharged (90% of its capacity) in 6 h.
- The combination of the two-hours linear ramp of temperature setpoint and PCM-HX can reduce by 14% energy consumption and achieve 4% peak load reduction (due to thermal load in daytime);
- Appropriate air stream trough air channels and start discharge time of the PCM-HX are two important factors toward achieving optimum performance of free cooling with PCM-HX. Correct implementation of these factors can reduce electric load fluctuation by 24%;

Results shows that the use of active PCM-HX for free cooling applications along with appropriate control strategies could be an effective solution to have better energy efficiency in buildings, reduce the sizing of the HVAC unit at the design stage, and reduce energy bills, thus reducing both operation and initial capital costs.

6. Chapter 6

6.1. Energy flexibility

Demand side response (DSR) is potential energy flexibility by end users and how it can provide value to the grid (Jensen, Marszal-Pomianowska et al. 2017). It can be in the form of system cost reduction, increasing system reliability or system size reduction. In this context, heating and cooling system, and potential storage of energy are most promising areas in building sector for demand response.

Flexibility is generally classified into two forms: (1) Explicit flexibility, and (2) Implicit flexibility. Explicit flexibility can provide flexibility in real time or on short notice and where the system is controllable. Implicit flexibility is related to a long-term expected reduction in load demand (e.g. changes in end user behavior).

There are six typical forms of DSR (WorldBank 2005) presented in Figure 6-1:

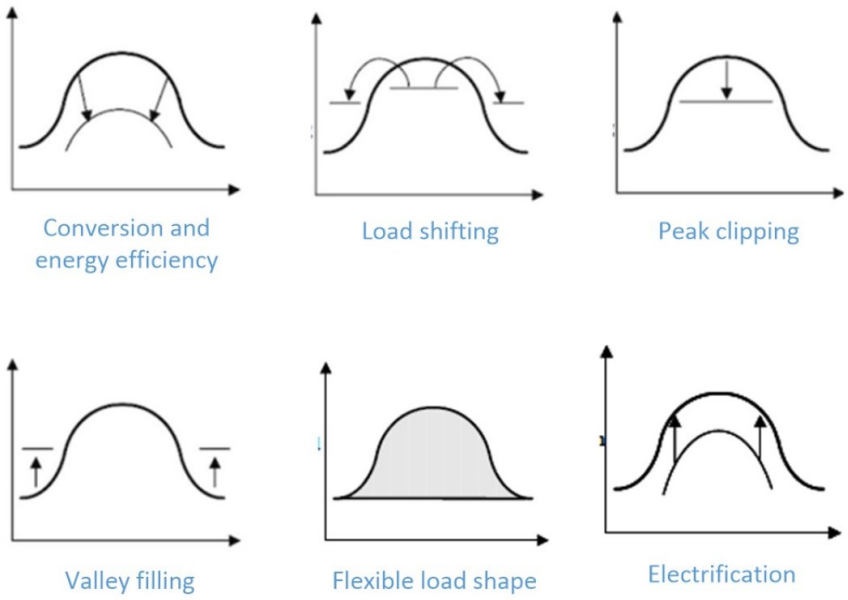

Figure 6-1. Demand side response(WorldBank 2005)

- **Conversion and energy efficiency:** includes long-term replacement of electricity with another energy carrier, or installing more efficient equipment;
- **Load shifting:** is the short-term shift of load peak load reduction, while consuming the same amount of energy over the day;
- **Peak clipping:** is peak load reduction without consuming the same amount of energy in other hours. This is achievable either by reducing comfort, or short-term replacement by other energy carriers;
- **Valley filling:** is exploiting unused capacity during off-peak hours (e.g. charging batteries or thermal energy storages)
- **Flexible load shape:** is making the load shape dynamically responsive to reliability conditions.
- **Electrification:** is increasing electricity demand, involves conversion from other energy sources to electricity.

The three first form of flexibility are of most interest, as the load reduction provides reducing capacity needs in the electrical grid.

6.2.**Time of use electricity rate**

The objective of this section is to show the potential of shifting the energy use from high to low price periods. Time-of-Use Pricing (Ontario Hydro Rates) will be used as an indicator of the price of electricity. These rates divided into three categories: off-peak, mid-peak and on-peak rate price. Figures 6-2 and 6-3 provides an overview of time-of-Use pricing in winter and summer, respectively.

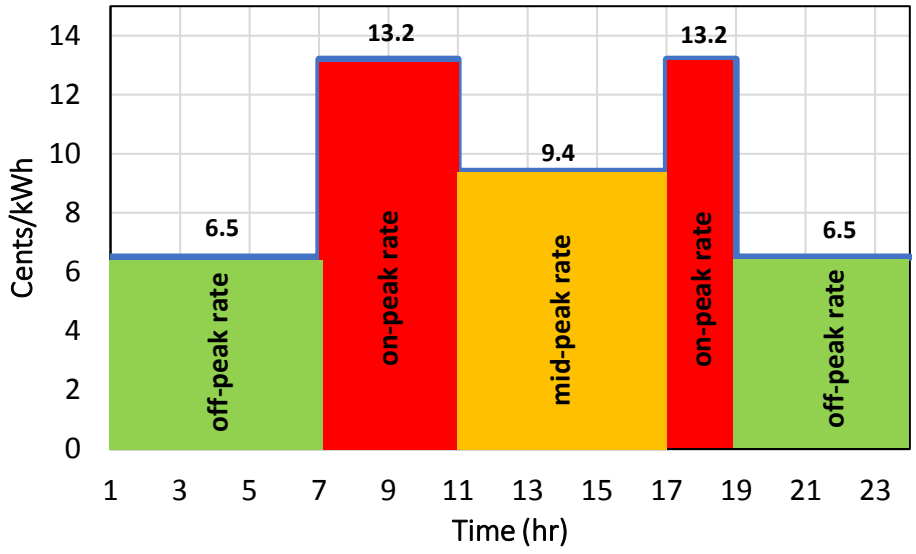

Figure 6-2. Time of use rate - winter rate

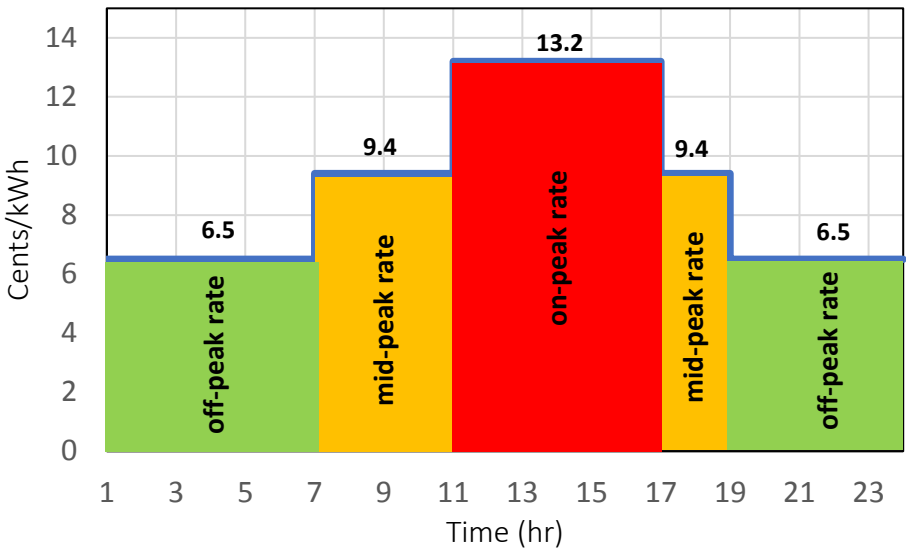

Figure 6-3. Time of use rate - summer rate

6.3. **Flexibility index**

Energy flexibility in buildings has been defined as "the possibility to deviate the electricity consumption of a building from the reference scenario at a specific point in time and during a certain time span" (Torres Ruilova 2017). In this section, a flexibility factor has been calculated based on Equation (11). This index shows the ability to shift the energy use from high to low price periods.

$$Flexibility\ factor = \frac{\int_{low\ price\ time} q_{heating}\,dt - \int_{high\ price\ time} q_{heating}\,dt}{\int_{low\ price\ time} q_{heating}\,dt + \int_{high\ price\ time} q_{heating}\,dt} \qquad (11)$$

where:

- Flexibility factor = 0: the heating/cooling use is similar in low and high price periods.
- Flexibility factor = 1: no heating/cooling is used in high price periods.
- Flexibility factor = -1: no heating/cooling is used in low price periods.

Table 6-1 provides a comparison between reference case study (without PCM-HX) and the case with PCM-HX and two-hour linear ramp for both summer and winter scenarios.

Table 6-1. Flexibility scenarios of the building

Case study	Mean power load during daytime (W)	Cooling power fluctuation (W) - daytime	Flexibility factor (–)
Summer			
Ref. case	629.17	410.22	-
With PCM-HX	370.90	312.15	0.2
Changes Relative to Ref. case	41 % reduction	24 % reduction	20 % increase
Winter	Mean power load during daytime (W)	Peak load (W)	Flexibility factor (–)
Ref. case	988	3000	0
With PCM-HX	775	1775	0.1
Changes Relative to Ref. case	22 % reduction	41% reduction	10 % increase

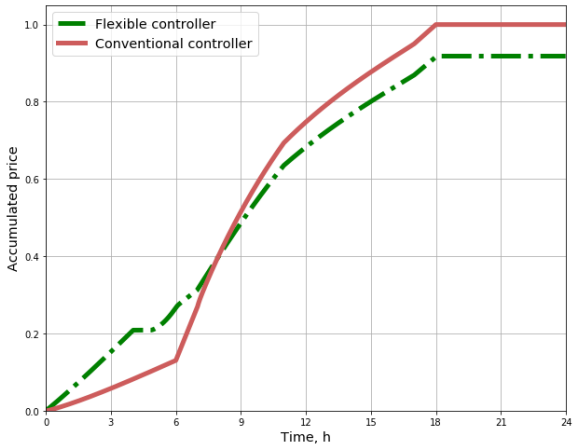

Figure 6-4. The accumulated penalty for each of the controllers – Heating season

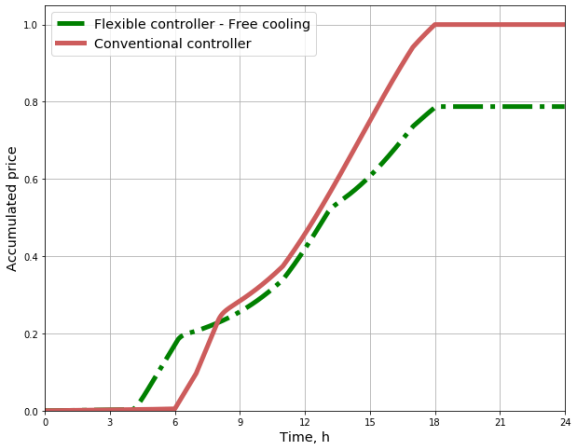

Figure 6-5. The accumulated penalty for each of the controllers – Cooling season

The results presented in Table 4 and Figures 6-4 and 6-5 show that such a PCM-HX along with appropriate control strategies could provide flexibility to the grid, reduce mean power load during daytime and peak power demand, simultaneously. The heating power can also be modulated between hours at medium price and hours at low price by storing heat in the thermal mass.

6.4. **Conclusion**

In this chapter, energy flexibility of a building equipped with PCM-HX and appropriate control strategies was evaluated. Results show:

- The energy consumption during the time of high price decreases by 30% in cooling season and 25 % during heating season.
- Mean power load during daytime is reduced by 41 % in free cooling application and 22 % in winter.
- Cooling power fluctuation is reduced by 24 % and 41 % during summer and winter respectively.
- And totally, flexibility factor increases by 20 % in summer and 10 % in winter.

Results show, such a PCM-HX along with appropriate control strategies could provide flexibility to the grid, reduce mean power load during daytime and peak power demand, simultaneously.

7. Chapter 7

7.1. Conclusion

In this thesis, the application of the PCM-HX device in order to reduce peak load and HVAC system size, and enhance energy flexibility in buildings was investigated. This study investigated different design options for the integration of active PCM-HX in an office zone. The charging and discharging of the PCM, arranged in layers, is managed by a controlled airflow passing through these layers. Several control strategies was also evaluated. The thermal behaviour of the PCM-HX in two design day scenarios has been studied: winter day (Heating purposes), and summer day (Free cooling purposes). Montreal climate conditions were used to evaluate the energy performance of the system.

This study presented the numerical modeling of the PCM-HX and its validation with experimental results. The Environmental Chamber of Concordia University was used as the case study for validation. The effect of thickness, length, number of the air channel, and airflow on the air temperature, and energy storage of the PCM-HX were evaluated. Results show:

- In turbulence air stream through PCM-HX, lower the airflow rate leads to the better performance of the system (in terms of energy consumption and noise).

- Although increasing the number of air channels in PCM-HX causes reducing energy per unit of volume, the charging and discharging time decreases and lead to faster and more easily controllable PCM-HX.

The integration of the proposed PCM-HX in an office zone was evaluated along with the effect of enhanced control strategies. Results shows that the use of active PCM-HX and appropriate control strategies could be an effective solution to have better energy flexibility in buildings, reduce the sizing of the HVAC unit at the design stage and to enhance energy cost reductions, thus possibly reducing both operation and initial capital costs.

The free cooling application of the PCM-HX was also investigated. It was found that combination of the two-hour linear ramp of temperature setpoint and PCM-HX can reduce by 14% energy consumption. Based on results appropriate airflow rate trough air channels and start discharge time of the PCM-HX are two important factors toward achieving optimum performance of free cooling with PCM-HX. Correct implementation of these factors can reduce electric load fluctuation by 24%;

Energy flexibility of a building equipped with PCM-HX was evaluated. Results show, the energy consumption during the time of high price decreases by 30% in cooling season and 25 % during heating season. It was also found, implementation of the PCM-HX could increase energy flexibility by 20 % in summer and 10 % in winter.

Results show, such a PCM-HX along with appropriate control strategies could provide flexibility to the grid, enhance energy efficiency in buildings and reduce peak power demand during high price hours, simultaneously.

7.2. **Contributions**

The main contributions of this thesis are as follows:

An evaluation was conducted on the PCM-HX with different design configurations toward achieving better performance of the device. It was demonstrated effect of each design configuration on the performance of the system.

The active PCM-HX integrated to the HVAC system under different control strategies in order to achieve peak load reduction, the optimal energy storage, and load shifting. This peak demand reduction may also enable smaller heating and cooling equipment and ducts, with a consequent reduction of system size and costs.

Free cooling application of the PCM-HX along with the effect of enhanced control strategies was evaluated. It was demonstrated that airflow rate through air channels and discharging start times of the PCM-HX are two important factors toward achieving best performance of free cooling with PCM-HX.

An investigation was done with the effect of the PCM-HX on enhancing the energy flexibility in buildings. Time-of-Use pricing was used as an indicator of the price of electricity and a flexibility factor was applied for analysis of the results.

7.3. **Suggestions for future work**

This thesis showed that airflow rate through air channels and discharging start times of the PCM-HX are two important factors toward achieving best performance of free cooling with PCM-HX. In a future work, the performance of the PCM-HX will be optimized for free-cooling

applications by applying a model predictive control (MPC) method to determine optimal flow rates and discharging start times.

Building-Integrated Photovoltaic and Thermal (BIPVT) is an energy generation system that incorporates solar PV panels to building. More research is necessary to integrate the BIPVT systems to the thermal energy storage device. The thermal management functionality of the presented PCM-HX could be a good solution for filling the gap between energy generation by BIPVT and energy consumption of the buildings.

Different weather conditions provide a variety of temperatures throughout the year. For most PCM systems phase change temperature will not appropriate for both summer and winter conditions. A solution can be using multilayered PCM systems (i.e. PCMs of different phase temperatures). A suggestion for further research into this field would be to investigate the PCM-HX with adjustable phase temperatures, which could be controlled as a part of an adaptive system.

8. References

Afroz, Z., G. Shafiullah, T. Urmee and G. Higgins (2017). "Modeling techniques used in building HVAC control systems: A review." Renewable and Sustainable Energy Reviews.

Arkar, C. and S. Medved (2007). "Free cooling of a building using PCM heat storage integrated into the ventilation system." Solar Energy 81(9): 1078-1087.

Arkar, C., B. Vidrih and S. Medved (2007). "Efficiency of free cooling using latent heat storage integrated into the ventilation system of a low energy building." International Journal of Refrigeration 30(1): 134-143.

Ascione, F., N. Bianco, R. F. De Masi, F. de'Rossi and G. P. Vanoli (2014). "Energy refurbishment of existing buildings through the use of phase change materials: Energy savings and indoor comfort in the cooling season." Applied Energy 113: 990-1007.

Athienitis, A., C. Liu, D. Hawes, D. Banu and D. Feldman (1997). "Investigation of the thermal performance of a passive solar test-room with wall latent heat storage." Building and environment 32(5): 405-410.

Barzin, R., J. J. Chen, B. R. Young and M. M. Farid (2016). "Application of weather forecast in conjunction with price-based method for PCM solar passive buildings–An experimental study." Applied Energy 163: 9-18.

Bastani, A., F. Haghighat and C. J. Manzano (2015). "Investigating the effect of control strategy on the shift of energy consumption in a building integrated with PCM wallboard." Energy Procedia 78: 2280-2285.

Berardi, U. and M. Manca (2017). "The energy saving and indoor comfort improvements with latent thermal energy storage in building retrofits in Canada." Energy Procedia 111: 462-471.

Berardi, U. and S. Soudian (2018). Benefits of latent thermal energy storage in the retrofit of Canadian high-rise residential buildings. Building Simulation, Springer.

Bigaila, E. and A. Athienitis (2017). "Modeling and simulation of a photovoltaic/thermal air collector assisting a façade integrated small scale heat pump with radiant PCM panel." Energy and Buildings 149: 298-309.

Bourne, S. and A. Novoselac (2015). Compact PCM-based thermal stores for shifting peak cooling loads. Building Simulation, Springer.

Bozkaya, B., R. Li, T. Labeodan, R. Kramer and W. Zeiler (2017). "Development and evaluation of a building integrated aquifer thermal storage model." Applied Thermal Engineering 126: 620-629.

Braun, J. E. and K.-H. Lee (2006). "An Experimental Evaluation of Demand Limiting Using Building Thermal Mass in a Small Commercial Building." ASHRAE transactions 112(1).

Butala, V. and U. Stritih (2009). "Experimental investigation of PCM cold storage." Energy and Buildings 41(3): 354-359.

Cabeza, L. F. (2008). Heat And Cold Storage With PCM: An Up To Date Introduction Into Basics And Applications. Heat and Mass Transfer, Springer.

Candanedo, J. A., V. R. Dehkordi, A. Saberi-Derakhtenjani and A. K. Athienitis (2015). "Near-optimal transition between temperature setpoints for peak load reduction in small buildings." Energy and Buildings 87: 123-133.

Childs, K. and T. Stovall (2012). "Potential energy savings due to phase change material in a building wall assembly: an examination of two climates." Oak Ridge National Laboratory, Oak Ridge, TN, Technical Report No. ORNL/TM-2012/6.

Crawley, D. B., L. K. Lawrie, C. O. Pedersen and F. C. Winkelmann (2000). "Energy plus: energy simulation program." ASHRAE journal 42(4): 49-56.

D'Angiolella, R., M. de Groote and M. Fabbri (2016). "NZEB 2.0: Interactive players in an evolving energy system." REHVA J 53: 52-55.

Dermardiros, V. (2015). Modelling and experimental evaluation of an active thermal energy storage system with phase-change materials for model-based control, Concordia University.

Dermardiros, V. and A. Athienitis (2015). Comparison of PCM-active thermal storage systems integrated in building enclosures. 10th Conference on Advanced Building Skins.

Dincer, I. and M. Rosen (2002). "Thermal energy storage (TES) methods." Thermal Energy Storage: Systems and Applications: 104-141.

Dincer, I. and M. Rosen (2002). Thermal energy storage: systems and applications, John Wiley & Sons.

Dolado, P., A. Lázaro, J. M. Marín and B. Zalba (2012). PCM-Air Heat Exchangers: Slab Geometry. Heat Exchangers-Basics Design Applications, InTech.

Du, K., J. Calautit, Z. Wang, Y. Wu and H. Liu (2018). "A review of the applications of phase change materials in cooling, heating and power generation in different temperature ranges." Applied Energy 220: 242-273.

DuPont (2/15/2019). "DuPont Energain - Energy-saving thermal mass systems." Availabe at: http://www.cse.fraunhofer.org/hs-fs/hub/55819/file-14736951-pdf/docs/energain_flyer.pdf

Farid, M. M., A. M. Khudhair, S. A. K. Razack and S. Al-Hallaj (2004). "A review on phase change energy storage: materials and applications." Energy conversion and management 45(9-10): 1597-1615.

Fleischer, A. S. (2015). Fundamental thermal analysis. Thermal Energy Storage Using Phase Change Materials, Springer: 75-85.

Gil, A., M. Medrano, I. Martorell, A. Lázaro, P. Dolado, B. Zalba and L. F. Cabeza (2010). "State of the art on high temperature thermal energy storage for power generation. Part 1—Concepts, materials and modellization." Renewable and Sustainable Energy Reviews 14(1): 31-55.

Givoni, B. (1984). "Options and applications of passive cooling." Energy and Buildings 7(4): 297-300.

Guarino, F., A. Athienitis, M. Cellura and D. Bastien (2017). "PCM thermal storage design in buildings: Experimental studies and applications to solaria in cold climates." Applied energy 185: 95-106.

Hed, G. and R. Bellander (2006). "Mathematical modelling of PCM air heat exchanger." Energy and Buildings 38(2): 82-89.

Heier, J., C. Bales and V. Martin (2015). "Combining thermal energy storage with buildings–a review." Renewable and Sustainable Energy Reviews 42: 1305-1325.

Jensen, S. Ø., A. Marszal-Pomianowska, R. Lollini, W. Pasut, A. Knotzer, P. Engelmann, A. Stafford and G. Reynders (2017). "IEA EBC annex 67 energy flexible buildings." Energy and Buildings 155: 25-34.

Klein, K., S. Herkel, H.-M. Henning and C. Felsmann (2017). "Load shifting using the heating and cooling system of an office building: Quantitative potential evaluation for different flexibility and storage options." Applied Energy 203: 917-937.

Kośny, J. (2015). Thermal and Energy Modeling of PCM-Enhanced Building Envelopes. PCM-Enhanced Building Components, Springer: 167-234.

Kuznik, F. and J. Virgone (2009). "Experimental investigation of wallboard containing phase change material: Data for validation of numerical modeling." Energy and Buildings 41(5): 561-570.

Le Dréau, J. and P. Heiselberg (2016). "Energy flexibility of residential buildings using short term heat storage in the thermal mass." Energy 111: 991-1002.

Lee, K.-h. and J. E. Braun (2008). "Model-based demand-limiting control of building thermal mass." Building and Environment 43(10): 1633-1646.

Manning, M., M. Swinton, F. Szadkowski, J. Gusdorf and K. Ruest (2005). "The Effects of Thermostat Setting on Seasonal Energy Consumption at the CCHT Research Facility." CCHT Report.

Mao, N., D. Pan, Z. Li, Y. Xu, M. Song and S. Deng (2017). "A numerical study on influences of building envelope heat gain on operating performances of a bed-based task/ambient air conditioning (TAC) system in energy saving and thermal comfort." Applied energy 192: 213-221.

Mao, N., M. Song, D. Pan, Z. Li and S. Deng (2017). "Numerical investigations on the effects of envelope thermal loads on energy utilization potential and thermal non-uniformity in sleeping environments." Building and Environment 124: 232-244.

Medved, S. and C. Arkar (2008). "Correlation between the local climate and the free-cooling potential of latent heat storage." Energy and Buildings 40(4): 429-437.

Moon, J. W. and S.-H. Han (2011). "Thermostat strategies impact on energy consumption in residential buildings." Energy and Buildings 43(2-3): 338-346.

Morovat, N. and A. K. Athienitis (2018). Impact of building-integrated PCM on the indoor thermal environment and energy performance of an office zone. 12th IIR Conference on Phase-Change Materials and Slurries for Refrigeration and Air Conditioning (PCM 2018). Orford (Québec), Canada: 8.

Mosaffa, A., C. I. Ferreira, F. Talati and M. Rosen (2013). "Thermal performance of a multiple PCM thermal storage unit for free cooling." Energy Conversion and Management 67: 1-7.

Narain, J., W. Jin, M. Ghandehari, E. Wilke, N. Shukla, U. Berardi, T. El-Korchi and S. Van Dessel (2015). "Design and application of concrete tiles enhanced with microencapsulated phase-change material." Journal of Architectural Engineering 22(1): 05015003.

Navarro, L., A. de Gracia, D. Niall, A. Castell, M. Browne, S. J. McCormack, P. Griffiths and L. F. Cabeza (2016). "Thermal energy storage in building integrated thermal systems: A review. Part 2. Integration as passive system." Renewable Energy 85: 1334-1356.

Nikoofard, S., V. I. Ugursal and I. Beausoleil-Morrison (2015). Techno-economic assessment of the impact of phase change material thermal storage on the energy consumption and GHG emissions of the Canadian Housing Stock. Building Simulation, Springer.

NRCan, O. (2006). "Energy Efficiency Trends in Canada, 1990-2003." Gatineau, QC.

Papachristou, A. C., C. A. Vallianos, V. Dermardiros, A. K. Athienitis and J. A. Candanedo (2018). "A numerical and experimental study of a simple model-based predictive control strategy in a perimeter zone with phase change material." Science and Technology for the Built Environment: 1-12.

Paris, J., M. Falardeau and C. Villeneuve (1993). "Thermal storage by latent heat: a viable option for energy conservation in buildings." Energy Sources 15(1): 85-93.

Pasupathy, A. and R. Velraj (2008). "Effect of double layer phase change material in building roof for year round thermal management." Energy and Buildings 40(3): 193-203.

Reynders, G. (2015). "Quantifying the impact of building design on the potential of structural storage for active demand response in residential buildings."

Reynders, G., R. A. Lopes, A. Marszal-Pomianowska, D. Aelenei, J. Martins and D. Saelens (2018). "Energy flexible buildings: An evaluation of definitions and quantification methodologies applied to thermal storage." Energy and Buildings.

Rodriguez-Ubinas, E., B. A. Arranz, S. V. Sánchez and F. N. González (2013). "Influence of the use of PCM drywall and the fenestration in building retrofitting." Energy and Buildings 65: 464-476.

Saffari, M., A. de Gracia, S. Ushak and L. F. Cabeza (2017). "Passive cooling of buildings with phase change materials using whole-building energy simulation tools: A review." Renewable and Sustainable Energy Reviews 80: 1239-1255.

Saman, W., F. Bruno and E. Halawa (2005). "Thermal performance of PCM thermal storage unit for a roof integrated solar heating system." Solar energy 78(2): 341-349.

Santamouris, M. and D. Asimakopoulos (1996). Passive cooling of buildings, James & James London.

Sharma, A., V. V. Tyagi, C. Chen and D. Buddhi (2009). "Review on thermal energy storage with phase change materials and applications." Renewable and Sustainable energy reviews 13(2): 318-345.

Soares, N., J. J. Costa, A. R. Gaspar and P. Santos (2013). "Review of passive PCM latent heat thermal energy storage systems towards buildings' energy efficiency." Energy and buildings 59: 82-103.

Soares, N., C. F. Reinhart and A. Hajiah (2017). Simulation-based analysis of the use of PCM-wallboards to reduce cooling energy demand and peak-loads in low-rise residential heavyweight buildings in Kuwait. Building Simulation, Springer.

Soudian, S. and U. Berardi (2017). "Experimental investigation of latent thermal energy storage in high-rise residential buildings in Toronto." Energy Procedia 132: 249-254.

Stetiu, C. and H. Feustel (1998). Phase-change wallboard and mechanical night ventilation in commercial buildings. Lawrence Berkeley National Laboratory, University of California; 1998, McGraw-Hill Int. Ed.

Stritih, U. (2003). "Heat transfer enhancement in latent heat thermal storage system for buildings." Energy and buildings 35(11): 1097-1104.

Stritih, U. and V. Butala (2007). "Energy saving in building with PCM cold storage." International journal of energy research 31(15): 1532-1544.

Stritih, U., V. Tyagi, R. Stropnik, H. Paksoy, F. Haghighat and M. M. Joybari (2018). "Integration of passive PCM technologies for net-zero energy buildings." Sustainable cities and society 41: 286-295.

Szokolay, S. (2012). Introduction to architectural science, Routledge.

Tabares-Velasco, P., C. Christensen and M. Bianchi (2012). "Simulated Peak Reduction and Energy Savings of Residential Building Envelope With Phase Change Materials." ASHRAE Trans 118(2): 90-97.

Torres Ruilova, B. (2017). "Evaluation of energy flexibility of buildings using structural thermal mass."

Touchie, M., K. Pressnail and E. Tzekova (2014). Assessing potential energy retrofits of multi-unit residential buildings in the Greater Toronto area. Proceedings of the 14th Canadian Conference on Building Science and Technology, Toronto, Canada.

Turnpenny, J., D. Etheridge and D. Reay (2000). "Novel ventilation cooling system for reducing air conditioning in buildings.: Part I: testing and theoretical modelling." Applied Thermal Engineering 20(11): 1019-1037.

Waide, P., J. Amann and A. Hinge (2007). "Energy efficiency in the north american existing building stock." Energy efficiency series.

Waqas, A. and Z. U. Din (2013). "Phase change material (PCM) storage for free cooling of buildings—a review." Renewable and sustainable energy reviews 18: 607-625.

WorldBank (2005). Primer on Demand-Side Management. http://siteresources.worldbank.org/INTENERGY/Resources/PrimeronDemand-SideManagement.pdf.

Yanbing, K., J. Yi and Z. Yinping (2003). "Modeling and experimental study on an innovative passive cooling system—NVP system." Energy and buildings 35(4): 417-425.

Yu, Z. J., G. Huang, F. Haghighat, H. Li and G. Zhang (2015). "Control strategies for integration of thermal energy storage into buildings: State-of-the-art review." Energy and Buildings 106: 203-215.

Zalba, B., J. M. Marın, L. F. Cabeza and H. Mehling (2003). "Review on thermal energy storage with phase change: materials, heat transfer analysis and applications." Applied thermal engineering 23(3): 251-283.

Zalba, B., J. M. Marín, L. F. Cabeza and H. Mehling (2004). "Free-cooling of buildings with phase change materials." International Journal of Refrigeration 27(8): 839-849.

Zhou, Z., Z. Zhang, J. Zuo, K. Huang and L. Zhang (2015). "Phase change materials for solar thermal energy storage in residential buildings in cold climate." Renewable and Sustainable Energy Reviews 48: 692-703.

Zhu, N., P. Hu, L. Xu, Z. Jiang and F. Lei (2014). "Recent research and applications of ground source heat pump integrated with thermal energy storage systems: A review." Applied thermal engineering 71(1): 142-151.

Zhu, N., Z. Ma and S. Wang (2009). "Dynamic characteristics and energy performance of buildings using phase change materials: a review." Energy Conversion and Management 50(12): 3169-3181.

9. Appendix

Code: PCM-HX in an office zone:

```
================================================================================
#  Prepared by Navid Morovat, (C) 2018-2019
================================================================================
# Load Dependencies:
import math
import numpy as np
import matplotlib.pylab as plt
import matplotlib as mpl
mpl.rc('figure', figsize=(8, 6))
import pandas as pd
================================================================================
# Capacitance as a function of temperature: Cp(T)
def fCp(Temp, skew, T_peak, rng, dh, Cp_avg):
    Tx = (Temp-T_peak)/rng
    return dh*mpl.mlab.normpdf(Tx,0,1)*(1+math.erf(skew*Tx/np.sqrt(2))) + Cp_avg
================================================================================
# U: Conductance matrix (symmetrical)
# C: Capacitance vector
# F: Conductance vector of nodes connected to a known temperature source
# T: Temperature vector
# q: Heat flow, only external sources
# Q: Heat flow vector, external sources + capacitance from previous timestep
# nN: Number of nodes
# VF: View factor matrix
# Node that indexing starts at "0" in python (not "1" like in Matlab)
# Node Number: Surface
# 0: left surface
# 1: right surface
# 2: back surface
# 3: front wall, top -> opaque
```

4: front wall, middle -> transparent

5: front wall, bottom -> opaque

6: floor surface

7: ceiling surface

8: air node

9: side inside; node connected to left and right surfaces

10: floor inside; node connected to ceiling inside

11: ceiling inside

12: back inside; behind of this layer considered adiabatic

13: middle window, outside pane

14: PCM, node, first set

15: PCM, surface, first set

16: PCM, air stream, first set

17: PCM, node, second set

18: PCM, surface, second set

19: PCM, air stream, second set

P0: air temp at inlet of PCM

P1: air temp after first set of PCM

P2: air temp after second set of PCM

==========

Geometry and other properties

A_sid = 12.8

A_cei = 16.0

A_bck = 12.8

A_ftp = 4.8

A_ftm = 4.8

A_fbt = 3.2

A = np.array([A_sid, A_sid, A_bck, A_ftp, A_ftm, A_fbt, A_cei, A_cei, 0, A_sid, A_cei, A_cei, A_bck, A_ftm])

Vol = 51.2

A_total = 2*(A_sid + A_bck + A_cei)

R_curt = 3. # m^2K/W

```
purge = 0       # nightime ventilation, on/off control

VF = np.array([ [0,        0.1827, 0.1491, 0.0685, 0.0685, 0.0457, 0.2429, 0.2429], \
            [0.1827,    0,      0.1491, 0.0685, 0.0685, 0.0457, 0.2429, 0.2429], \
            [0.1766,    0.1766, 0,      0.0662, 0.0662, 0.0442, 0.2350, 0.235],  \
            [0.1827,    0.1827, 0.1491, 0,      0,      0,      0.2429, 0.2429], \
            [0.1827,    0.1827, 0.1491, 0,      0,      0,      0.2429, 0.2429], \
            [0.1827,    0.1827, 0.1491, 0,      0,      0,      0.2429, 0.2429], \
            [0.1944,    0.1944, 0.1588, 0.0729, 0.0729, 0.0486, 0,      0.2582], \
            [0.1944,    0.1944, 0.1588, 0.0729, 0.0729, 0.0486, 0.2582, 0] ])
nR = np.size(VF,0)
==========================================================================

# Radiosity
sig = 5.67e-8
e_surf = 0.9
e_glas = 0.868
e_lowe = 0.013
emis = np.ones((nR,1))*e_surf   # emissivity vector
emis[4] = e_glas
uRad = np.zeros((nR,nR))
for iR in range(0,nR):
    for jR in range(0,nR):
        if VF[iR,jR] != 0:
            uRad[iR,jR]    =    ((1-emis[iR])/(A[iR]*emis[iR])    +    1/(A[iR]*VF[iR,jR])    +    (1-
emis[jR])/(A[jR]*emis[jR]))**-1
==========================================================================

#%%
# Solar radiation
#with open('direct.pkl') as f:
#with open('direct_60.pkl') as f:
    #q_st, q_sa_ext_pane, q_sa_int_pane = pickle.load(f)
data  =  pd.read_csv('F:\PCM  Journal/qin.csv',  parse_dates=True,  infer_datetime_format=True,
index_col=0)
```

```
q_st = data['q_st'].values
q_sa_ext_pane = data['q_sa_ext_pane'].values
q_sa_int_pane = data['q_sa_int_pane'].values
# Overcast
q_st_overcast = 0.20 * q_st
# Assume Overcast sky
q_st = q_st_overcast
q_sa_ext_pane = 0.20*q_sa_ext_pane
q_sa_int_pane = 0.20*q_sa_int_pane
plt.figure()
plt.plot(q_st,'b', label='q_st')
plt.plot(q_sa_ext_pane,'g', label='q_sa_ext_pane')
plt.plot(q_sa_int_pane,'r', label='q_sa_int_pane')
plt.xlabel('Timestep')
plt.ylabel('Heat, W')
plt.legend(loc='best')
plt.grid()
plt.show()
#%%
# ASHRAE values; h-values are convection, conduction and radiation combined
h_out = 34.     # W/m^2K
#h_gap = 3.35    # W/m^2K
h_int = 4.      # W/m^2K
#k_gla = 1.      # W/mK
#x_gla = 0.004   # m; thickness of glass 4 mm
h_gap_conv = 1.50

# Material properties
# Concrete
k_conc = 1.731       # W/(m*K)
rho_conc = 2240      # kg/m^3
Cp_conc = 840        # J/(kg*K) where J = kgm^2/s^2
dx_conc = 0.050/2    # m, effective slab thickness 50 mm (2"), split into 2 nodes
```

```
# Gypsum
k_gyps = 0.810       # W/(m*K)
rho_gyps = 1680      # kg/m^3
Cp_gyps = 840        # J/(kg*K) where J = kgm^2/s^2
dx_gyps = 0.025      # m, 2 layers of gympsum 25 mm total (1"), 1 node

# Air
k_air = 0.0255       # W/(m*K)
rho_air = 1.184      # kg/m^3
Cp_air = 1006        # J/(kg*K)
multi = 20.          # Mass multiplier

# DuPont Energain PCM
use_PCM = True    # use the PCM-TES Option?
time_on_PCM = 6     # time to turn On PCM-TES system
time_off_PCM = 15.   # time to turn Off PCM-TES system
toggle = 0          # toggle "1" or "on" for PCM-TES fan to be active, "0" otherwise
k_PCM = 0.20         # W/(m*K)
rho_PCM = 850.       # kg/m^3
dx_PCM = 0.0052      # m
T_PCM = 28.          # degC, PCM-TES temperature when fully charged (hot)
h_PCM = 18.          # W/m^2K, convection in PCM-TES channel
n_PCM = 16           # number of PCM panels * 2
m_PCM = 50./3600.    # kg/s, massflow rate per PCM
m_PCM_total = n_PCM*m_PCM   # kg/s, total massflow rate in PCM-TES
A_PCM = 2.4        # m^2, area of PCM panel
ehAmCp = np.exp(-h_PCM*2*6*A_PCM/(10*m_PCM*Cp_air))
# Melting Cp Parameters
PCMm_skew = -10.     # skew
PCMm_T_peak = 23.6   # peak phase change temperature, C
PCMm_rng = 4.5       # range of phase change, C
PCMm_dh = 13100.     # enthalpy of phase change, J/kg 13100
```

```
PCMm_Cp_avg = 3500.  # average solid/liquid specific heat (full quality), J/kg
# Freezing Cp Parameters
PCMf_skew = -4.
PCMf_T_peak = 20.8
PCMf_rng = 4.68
PCMf_dh = 12600.
PCMf_Cp_avg = 3500.
=====================================================================

# Simulation control
nN = 20
st = 60         # steps per hour
H = 24          # hr; number of hours simulated
nt = int(st*H)  # number of timesteps-1
dt = 3600/st    # s (3600 sec = 1 hour)
days = 1        # number of days simulated
maxItt = 1.    # maximum number of iterations
maxErr = 1e-5   # maximum temperature difference from iteration to the next
critical_dt = rho_conc * Cp_conc*(dx_conc/2)**2/(2*k_conc)
print ("The critical timestep is: %0.f sec, while the selected timestep is: %.0f sec" %(critical_dt,
dt))

# Known temperatures
T_out = np.zeros((nt*days,1))   # degC
T_out_m = -15.                  # degC; Exterior temperature
dT_out = 10.
T_out_theta = -5*np.pi/4
w = 2*np.pi/86400

# Temperature setpoint
# Heating
T_SP = np.zeros((nt,1))         # degC; Interior temperature setpoint per timestep Heating
T_SP_day = 22.
T_SP_dT = 4.
```

```
setback_beg = 18.
setback_end = 6.
ramp_dur = 0                # hours
for t in range(0,nt):
    time = t*dt/3600.
    if (setback_beg <= time and time < (setback_beg+ramp_dur)):          # begin setback
        T_SP[t] = T_SP_day - (time-setback_beg)*T_SP_dT/ramp_dur
    elif ((setback_beg+ramp_dur) <= time or time < (setback_end-ramp_dur)): # night time
        T_SP[t] = T_SP_day - T_SP_dT
    elif ((setback_end-ramp_dur) <= time and time < setback_end):        # revert setback
        T_SP[t] = T_SP_day - (setback_end-time)*T_SP_dT/ramp_dur
    else:                                                # day time
        T_SP[t] = T_SP_day

# Cooling
T_SP_Cool = np.zeros((nt,1))    # degC; Interior temperature setpoint per timestep Cooling
T_SP_day_Cool = 24.
T_SP_dT_Cool = -2.
setback_beg_Cool = 18.
setback_end_Cool = 6.
ramp_dur_Cool = 0.          # hours
for t in range(0,nt):
    time = t*dt/3600.
    if (setback_beg_Cool <= time and time < (setback_beg_Cool+ramp_dur_Cool)):
        T_SP_Cool[t] = T_SP_day_Cool - (time-
setback_beg_Cool)*T_SP_dT_Cool/ramp_dur_Cool
    elif ((setback_beg_Cool+ramp_dur_Cool) <= time or time < (setback_end_Cool-
                ramp_dur_Cool)):
        T_SP_Cool[t] = T_SP_day_Cool - T_SP_dT_Cool
    elif ((setback_end_Cool-ramp_dur_Cool) <= time and time < setback_end_Cool):
        T_SP_Cool[t] = T_SP_day_Cool - (setback_end_Cool-
time)*T_SP_dT_Cool/ramp_dur_Cool
    else:
```

```
        T_SP_Cool[t] = T_SP_day_Cool
T_Setpoint_Heating = np.tile(T_SP,(days,1))
T_Setpoint_Cooling = np.tile(T_SP_Cool,(days,1))
# Heating/Cooling system
q_aux = np.zeros((nt*days,1))   # W
SP_Err = np.zeros((nt*days,1))  # degC
max_Cap = 3000.                 # W; Heater size
min_Cap = 0                  # W; minimum heat
Kp = max_Cap/0.5
Ki = 0.
iTerm = 0.
delay_nt = 5
heat_output = np.zeros((delay_nt,1))
heat_aux = 0.
SP_Err_Cool = np.zeros((nt*days,1))  # degC
max_Cap_Cool = 3000.
min_Cap_Cool = 0.
Kp_Cool = max_Cap_Cool/2
Ki_Cool = 0.0
iTerm_Cool = 0.
cool_aux = 0.
```

==========

```
#%%
# Declare variables
C = np.zeros((nN,1))        # J/K
T = np.zeros((nt*days,nN))  # degC
P0 = np.zeros((nt*days,1))  # degC
P1 = np.zeros((nt*days,1))  # degC
P2 = np.zeros((nt*days,1))  # degC
q_PCM = np.zeros((nt*days,1))

# Nodes with capacitance
C[8] = rho_air*Cp_air*(Vol*multi)
```

```
C[9] = rho_gyps*Cp_gyps*(dx_gyps*A[9])
C[10] = rho_conc*Cp_conc*(2*dx_conc*A[10])
C[11] = rho_conc*Cp_conc*(2*dx_conc*A[11])
C[12] = rho_gyps*Cp_gyps*(dx_gyps*A[12])

# Initial condition
#T[0,] = 20.
T[0,] = T_SP_day - T_SP_dT
================================================================================
#%%
# Loop for number of days
  # Loop for all time in a day
for d in range(0,days):
    # Loop for all time in a day
    for t in range(0,nt):
        Itt = 1.
        Err = 100.
        Tp = T[d*nt+t,]
        print ("Tpis :", Tp)
        time = t*dt/3600.
        # Turn on PCM-TES system
        if (use_PCM == True and time >= time_on_PCM  and time < time_off_PCM and toggle ==
                    0):
            toggle = 1
            T[d*nt+t,14:20] = T_PCM      # re-initialize temperatures
        # Turn off PCM-TES system
        if (use_PCM == True and time >= time_off_PCM and toggle == 1):
            toggle = 0
        while(Itt <= maxItt and Err > maxErr):
            # Declare variables
            U = np.zeros((nN,nN))       # W/K
            F = np.zeros((nN,1))        # W/K
            #TK = np.zeros((nt*days,1))
```

```
# How are the nodes connected?
# Radiation exchange between inside surfaces
TR = T[d*nt+t,] + 273
for jR in range(0,nR):
    for iR in range(0,jR):
        if uRad[iR,jR] != 0:
            U[iR,jR] = sig*uRad[iR,jR]*(TR[iR]**4-TR[jR]**4) / (TR[iR]-TR[jR])
i_NaN = np.isnan(U)     # if both surfaces are at the exact same temperature,
U[i_NaN] = 0            # replace NaN with 0: no heat transfer bet surfaces
del i_NaN, iR, jR
# Radiation exchange between glass panes
h_gap_mid_rad = sig*(TR[4]**2+TR[13]**2)*(TR[4]+TR[13]) / (1/e_glas+1/e_lowe-1)
# Connected to air node
for i in range(0,8):
    U[i,8] = (1/(h_int*A[i]))**-1

# Side walls
U[0,9] = (dx_gyps/(2*k_gyps*A[0]))**-1
U[1,9] = (dx_gyps/(2*k_gyps*A[1]))**-1
# Floor and ceiling
U[6,10] = (dx_conc/(k_conc*A[6]))**-1
U[7,11] = (dx_conc/(k_conc*A[7]))**-1
#U[10,11] = (dx_conc/(k_conc*A[10]))**-1
# Back wall
U[2,12] = (dx_gyps/(2*k_gyps*A[2]))**-1
# Window, middle
h_gap_mid = h_gap_conv + h_gap_mid_rad
U[4,13] = (1/(h_gap_mid*A[4]))**-1

# Connected to temperature sources
F[3] = (1/(h_out*A[3]) + R_curt/A[3])**-1
F[5] = (1/(h_out*A[5]) + R_curt/A[5])**-1
F[8] = ACH*Vol*rho_air*Cp_air/3600
```

```
        F[13] = (1/(h_out*A[4]))**-1
        # PCM-TES
        U[14,15] = 2*A_PCM*k_PCM/dx_PCM     # first set
        U[15,16] = A_PCM*h_PCM
        U[17,18] = 2*A_PCM*k_PCM/dx_PCM     # second set
        U[18,19] = A_PCM*h_PCM
        C[14] = rho_PCM*A_PCM*dx_PCM*fCp(T[d*nt+t,14], PCMf_skew, PCMf_T_peak, PCMf_rng,PCMf_dh, PCMf_Cp_avg)
        C[17] = rho_PCM*A_PCM*dx_PCM*fCp(T[d*nt+t,16], PCMf_skew, PCMf_T_peak, PCMf_rng,PCMf_dh, PCMf_Cp_avg)
        P0[d*nt+t] = T[d*nt+t,8]
        P1[d*nt+t] = P0[d*nt+t]*ehAmCp + T[d*nt+t,15]*(1-ehAmCp)
        P2[d*nt+t] = P1[d*nt+t]*ehAmCp + T[d*nt+t,18]*(1-ehAmCp)
        q_PCM[d*nt+t] = toggle*m_PCM_total*Cp_air*(P2[d*nt+t]-P0[d*nt+t])
        print("q PCM is: ", P1)

        # U-matrix and its inverse
        Ue = U + U.T
        #print(U)
        # U is symmetrical, non-diagonals are -ve
        s = -np.sum(Ue,1)
        for i in range(0,nN):
           Ue[i,i] = s[i] - np.sum(F[i,]) + C[i]/dt
        del i, s
        Und = U + U.T
        #print ("U =",U)

        # Auxiliary heat, PI control
        errHeatSP = T_Setpoint_Heating[d*nt+t] - T[d*nt+t,8]
        errCoolSP = T[d*nt+t,8] - T_Setpoint_Cooling[d*nt+t]
        err = 0.5*(abs(errHeatSP)+errHeatSP) - 0.5*(abs(errCoolSP)+errCoolSP)
        #SP_Err[d*nt+t] = (np.abs(T_SP[t]-T[d*nt+t,8]) + (T_SP[t]-T[d*nt+t,8]))/2
        #iTerm += Ki*SP_Err[d*nt+t]
```

```
output = Kp*err #+ iTerm
if output > max_Cap:
   #iTerm -= output - max_Cap
   output = max_Cap
if output < min_Cap:
   #              iTerm += min_Cap - output
   output = min_Cap
heat_output[-1] = output
heat_aux = heat_output[-1] #np.mean(heat_output)

# Heat flow into the node

T_out[d*nt+t] = T_out_m + dT_out/2*np.cos(w*t*dt + T_out_theta)     # Outside
TK = T_out

q = np.zeros((nN,1)) # =Qin in 1.2 file jupyter notebook
q[0] = A[0]/(A[0]+A[1]+A[2]) * 0.30 * (A[4]*q_st[t]) # 30% of total solar
                                                    radiation falls on sides walls
q[1] = A[1]/(A[0]+A[1]+A[2]) * 0.30 * (A[4]*q_st[t]) # 30% of total solar
                                                   radiation falls on sides walls
q[2] = A[2]/(A[0]+A[1]+A[2]) * 0.30 * (A[4]*q_st[t]) # 30% of total solar
                                                   radiation falls on sides walls
q[3] = F[3]*T_out[d*nt+t]
q[4] = A[4]*q_sa_int_pane[t]
q[5] = F[5]*T_out[d*nt+t]
q[6] = 0.70 * (A[4]*q_st[t])    # 70% of total solar radiation falls on floor
q[8] = heat_aux - cool_aux + q_int[t] + q_PCM[d*nt+t]
q[10] = 0.                  # Heated floor, off
q[11] = 0.                  # Radiant ceiling, off
q[13] = A[13]*q_sa_ext_pane[t] + F[13]*T_out[d*nt+t]
q[16] = -m_PCM*Cp_air*(P1[d*nt+t]-P0[d*nt+t])
q[19] = -m_PCM*Cp_air*(P2[d*nt+t]-P1[d*nt+t])
# Q-vector
```

```
        #Q = np.zeros((nN,1))
        #for i in range(0,nN):
            #Q[i] = q[i] + C[i]*T[d*nt+t,i]/dt
        #del i
        #print ("QQ is :", Q)
        #Qin = np.zeros((nN,1))
        print ("q = " ,q)
#         Q = np.zeros((nN,1))
#         #Q = q + np.reshape(np.dot(F, TK[d*nt+t,]),(nN,1))
#         #print ("Q = " , Q)
#         for i in range(0,nN):
#             Q[i] = q[i] + C[i]*T[d*nt+t,i]/dt
#         del i
        Q = q + np.reshape(np.dot(F, TK[d*nt+t,]),(nN,1))


        # Compute temperature
        if (days*nt) > (d*nt+t+1):
            for c in range(nN):
                if (C[c] != 0):
                    T[d*nt+t+1,c] = dt/C[c] * (np.dot(Ue[c,],T[d*nt+t,]) + Q[c])
                else:
                    T[d*nt+t+1,c] = (np.dot(Und[c,],T[d*nt+t,]) + np.dot(F[c,],TK[d*nt+t,]) + q[c])/(np.sum(Und[c,]) + np.sum(F[c,]))
             # Store auxilary heat data
            q_aux[d*nt+t+1,] = heat_aux - cool_aux
            if heat_aux > 20 and cool_aux > 20:
                print ("Both heating and cooling are on at timestep: %i, heating: %.0f W, cooling: %.0f W" % (d*nt+t, heat_aux, cool_aux))
        # Compute iteration error
            Err = np.max(np.abs(T[d*nt+t+1,]-Tp))
            Tp = T[d*nt+t+1,]
        # Iterate
        Itt += 1
```

```
            if Itt == maxItt:
                print ("Max iteration occured at timestep: %i" % (d*nt+t))

               # T[d*nt+t+1,] = np.linalg.solve(U,Q).T
                #else:
                    #T[t+1,c] = (np.dot(U[c,],T[t,]) + (q[c,])/(np.sum(U[c,]) + np.sum(F[c,]))
        # Adjust heat output delay: move everything up by a timestep, add a 0 at the end
        heat_output = np.append(heat_output[-(delay_nt-1):],0)
print ("done")
==========================================================================
#%%
# Setpoints with internal temperature
fig = plt.figure()
ax = fig.add_subplot(1,1,1)
plt.hold(True)
plt.plot(np.dot(dt/3600.,range(0,nt)),T_SP,'k--', linewidth=3)
plt.plot(np.dot(dt/3600.,range(0,nt)),T_SP_Cool,'k:', linewidth=3)
plotT = T[(days-1)*nt:(days)*nt:]
plt.plot(np.dot(dt/3600.,range(0,nt)),plotT[:,8],'k', linewidth=3)
plt.xlim([0,2])
ticks = np.arange(0,25,3)
ax.set_xticks(ticks)
plt.ylim([15,28])
plt.grid()
plt.legend(['Heating setpoint','Cooling setpoint','Room air'], loc='lower right', fontsize='medium')
plt.xlabel('Time, h')
plt.ylabel('Temperature, degC')
plt.title('Zone Temperature')
==========================================================================
# Heating/cooling
plotQ = q_aux[(days-1)*nt:(days)*nt:]
print ("plotQ = ", plotQ)
fig = plt.figure()
```

```
ax = fig.add_subplot(1,1,1)
plt.hold(True)
plt.plot(np.dot(dt/3600.,range(0,nt)),plotQ,'k', linewidth=3)
plt.xlim([0,24])
ticks = np.arange(0,25,3)
ax.set_xticks(ticks)
plt.xlabel('Time, h')
plt.ylabel('Auxiliary Heat or Cooling, W')
plt.title('Auxiliary heating or cooling supplied to air node')
plt.grid(True)
plt.show()
#fig.savefig('test.eps')
#fig = plt.figure()
#plt.plot(q_aux)
#plt.ylim([-2000,1100])
```

==========

```
#%%
## Outside temperature
plotTout = T_out[(days-1)*nt:(days)*nt:]
fig = plt.figure()
ax = fig.add_subplot(1,1,1)
plt.hold(True)
plt.plot(np.dot(dt/3600.,range(0,nt)),plotTout, 'k', linewidth=3)
plt.xlim([0,24])
ticks = np.arange(0,25,3)
ax.set_xticks(ticks)
ax2 = ax.twinx()
ticks2 = np.arange(0,25,3)
ax2.set_xticks(ticks2)
ax2.plot(np.dot(dt/3600.,range(0,nt)),q_st*5,'y--', linewidth=3)
ax2.set_ylim(0, 120)
ax.set_ylim(-20,-8)
ax.set_xlabel('Time, h')
```

```
ax.set_ylabel('Outside temperature, degC')
ax2.set_xlabel('Time, h')
ax2.set_ylabel('Solar')
#plt.xlabel('Time, h')
plt.ylabel('Irradiance on the south facing façade, W/M^2')
lns1 = plt.plot(plotTout, 'k',label = 'Outside temperature')
lns2 = ax.plot( q_st*5,'y--', label = 'Irradiance - south facing facade')
lns = lns1+lns2
labs = [l.get_label() for l in lns]
ax.legend(lns, labs, loc=0)
#plt.title('Outside temperature')
ax.grid(True)
plt.show()
##fig.savefig('test.eps')
```

==========

```
#%%
## Solar radiation transmitted
fig = plt.figure()
ax = fig.add_subplot(1,1,1)
plt.hold(True)
#plt.plot(np.dot(dt/3600.,range(0,nt)),[q_st, q_sa_ext_pane],'y', linewidth=2)
plt.plot(np.dot(dt/3600.,range(0,nt)),q_st,'k', linewidth=3)
plt.plot(np.dot(dt/3600.,range(0,nt)),q_sa_int_pane,'k--', linewidth=3)
plt.plot(np.dot(dt/3600.,range(0,nt)),q_sa_ext_pane,'k:', linewidth=3)
plt.xlim([0,24])
ticks = np.arange(0,25,3)
ax.set_xticks(ticks)
plt.xlabel('Time, h')
plt.ylabel('Irradiance, W/m^2')
plt.legend(['Transmitted', 'Absorbed Interior Pane', 'Absorbed Exterior Pane'],loc='best', fontsize='medium')
plt.title('Solar Radiation')
plt.grid(True)
```

```
plt.show()
##fig.savefig('test.eps')
=============================================================================
#%%
plotT = T[(days-1)*nt:(days)*nt:]
fig = plt.figure()
ax = fig.add_subplot(1,1,1)
plt.hold(True)
plt.plot(np.dot(dt/3600.,range(0,nt)),plotT[:,[0,1,2,6,7,10,11]])
plt.xlim([0,24])
#plt.ylim([19.2,20])
ticks = np.arange(0,25,3)
ax.set_xticks(ticks)
plt.xlabel('Time, h')
plt.ylabel('Temperature, degC')
plt.title('Office temperature: periodic steady state')
plt.grid(True)
plt.legend(['Left Surface', 'Right Surface', 'Back Surface', 'Floor Surface',\
        'Ceiling Surface','Floor Inside','Ceiling Inside'],loc=0)
plt.show()
=============================================================================
```